Constructing Earth Formation History Using Deep Mantle Noble Gas Reservoirs

VINCENT SAVIGNAC (D1, 2 AND EVE J. LEE (D1, 2

¹Department of Astronomy & Astrophysics, UC San Diego, La Jolla, CA, 92093-0424, USA ²Department of Physics, McGill University, 3600 rue University, Montreal, QC, H3A 2T8, Canada

ABSTRACT

Noble gases are powerful probes of the Earth's early history, as they are chemically inert. Neon isotopic ratios in deep mantle plumes suggest that nebular gases were incorporated into the Earth's interior. This evidence implies the Earth's formation began when there was still gas around, with Earth embryos accreting primordial gas and a fraction of that gas dissolved into molten magma. In this work, we examine these implications, simulating the growth of primordial envelopes using modern gas accretion schemes, and computing the dissolution of nebular Ne into magma oceans following chemical equilibrium. We find that the embryo mass that reproduces the deep mantle concentration of primordial Ne is tightly constrained to $\sim 0.3 M_{\oplus}$, within a solar nebula depleted by $\geq 100 \times$ in gas density. Embryos of smaller masses cannot accrete enough gas to allow the mantle to reach the melting temperature of basalt. Embryos of larger masses accrete way too much gas, producing excessive Ne concentrations in the deep mantle. Based on our calculations, we suggest that the Earth's formation began with the assembly of $\sim 0.3 M_{\oplus}$ embryos during the dispersal of the solar nebula. Light noble gases (He, Ne) in the deep mantle reflect the primordial gas accretion history of the Earth, while heavy noble gases (Ar, Kr, Xe) probe early solid accretion processes. Our results are consistent with the final assembly of the Earth through at least two giant impacts after the dispersal of the nebula.

1. INTRODUCTION

Noble gases are direct geochemical probes of the Earth's early accretion processes because of their limited interactions with other elements. Their chemical inertness allows them to be transported through planetary interiors without altering the gas composition, making them ideal tracers of volatile delivery. Noble gas reservoirs can be found in different layers of the inner Earth (e.g., B. Marty 2012; A. N. Halliday 2013), with trace amounts detectable at the surface (atmosphere plus continental crust), in mid-ocean ridge basalts (MORB; degassed upper mantle), and in ocean island basalts (OIB; deep mantle plumes). Furthermore, non-radiogenic isotopes of noble gases (e.g., ³He, ²²Ne, ³⁶Ar, ⁸⁴Kr, and ¹³⁰Xe) trapped in MORB and OIB samples are not produced by radioactive decay and do not themselves undergo decay on timescales relevant to planetary evolution, which implies their existence since the formation of the solar system (e.g., M. Trieloff & J. Kunz 2005). Measuring the isotopic ratios of non-radiogenic species found in MORB and OIB samples is therefore a pow-

Email: vsavignac@ucsd.edu

erful tool for assessing the origin of these gases in the Earth's mantle and the accretion history of the planet.

However, the origin of the deep mantle noble gas reservoirs remains debated (see, e.g., J. M. Day et al. 2022, for a review), with three main possible explanations for their abundances. First, the nebular capture hypothesis suggests that the formation of Earth embryos in the early presence of the solar nebula would have led to the capture of primordial gas (H. Mizuno et al. 1980; Y. Abe & T. Matsui 1985; S. Sasaki & K. Nakazawa 1990). A proto-atmosphere, accreted early in the primordial solar nebula, could have dissolved a fraction of its gas into the hot, molten surface of planetary embryos. Second, solar-wind-irradiated (SWI) materials, that is, solids enriched with solar-wind ions, were incorporated into the Earth in the early stages of the solar system (M. Trieloff et al. 2000; C. J. Ballentine et al. 2005; A. Raquin & M. Moreira 2009; A. Colin et al. 2015; M. Moreira & S. Charnoz 2016; S. Peron et al. 2016, 2018). In fact, S. Peron et al. (2017) showed by comparing samples of irradiated lunar soil with MORB samples that the upper mantle reservoirs of Ne, He and possibly H are expected to be of SWI origin. Finally, carbonaceous chondrites (type CI), which are primitive meteorites rich in volatile elements (L. Alaerts et al. 1979a,b; G. W. Kallemeyn & J. T. Wasson 1981; R. Wieler et al. 1991, 1992; G. R.

Huss et al. 1996; H. Busemann et al. 2000), may also explain the noble gas reservoirs of the deep mantle, assuming they were incorporated into the Earth's interior during its assembly (G. Holland et al. 2009; B. Marty 2012; A. N. Halliday 2013).

For an imprint of these initial reservoirs to remain measurable in the mantle, all three scenarios require limited interactions between the mantle and the atmosphere. However, the subduction of atmospheric material from the oceanic lithosphere to the mantle is an efficient carrier of the heavier noble gases (S. Peron & S. Mukhopadhyay 2022). As a result, the Kr and Xe mantle budget suffers from significant atmospheric contamination, limiting studies of the origins of the initial Kr and Xe reservoirs (C. J. Ballentine & D. N. Barfod 2000; S. Mukhopadhyay & R. Parai 2019). Lighter noble gases such as He and Ne do not show traces of subducted atmospheric material (M. A. Kendrick et al. 2018), as their poor solubility from the atmosphere into seawater (R. Sander 2015) hinders their transfer from the oceanic lithosphere to the interior. Consequently, He and Ne offer the most promising avenue for unveiling the imprint of early accretion processes in the deep mantle.

Recent measurements of the non-radiogenic isotopes of Ne (²⁰Ne and ²²Ne) are beginning to shed light on the origin of deep mantle noble gas reservoirs. In their comparison of Galápagos samples with the depleted MORB mantle using a two-component mixing array, C. D. Williams & S. Mukhopadhyay (2019) retrieved a 20 Ne/ 22 Ne isotopic ratio of 13.23 ± 0.22 for the deep mantle reservoirs (see their figure 3). This value is statistically indistinguishable from the nebular capture expectation of 13.36 ± 0.18 (V. S. Heber et al. 2012), and deviates by more than 3σ from the $^{20}\text{Ne}/^{22}\text{Ne}$ ratios expected from atmospheric contamination, CI carbonaceous chondrites, or even SWI materials of 9.80 ± 0.01 , 10.67 ± 0.02 , and 12.5 ± 0.2 , respectively (values taken from Table 1 of B. Marty 2022). These measurements present a strong argument for a Ne reservoir in the deep mantle dominated by primordial nebular gas.

A reservoir of nebular gas in the interior of the Earth has strong implications for its formation history. The first one is that Earth embryos must have emerged when the gaseous solar nebula was still around, suggesting that the formation of the Earth happened early with the accretion of primordial atmospheres. Furthermore, the capture of volatiles in the planetary interior necessitates an exchange of gas between gas envelopes and planetary mantles via dissolution, requiring the presence of liquid magma oceans at the mantle-envelope boundary. Planetary embryos must therefore have been sufficiently massive for the accretion of an atmosphere and for their

rocky interior to have a molten outer layer. The cooling of the accreted gas sets the thermal conditions at the base of the atmosphere, which in turn control how much of the atmospheric volatiles are incorporated into the mantle through the atmosphere-mantle interface. For that reason, realistic envelope formation models in the nebula are required to accurately link the formation environment of protoplanets to their interior reservoirs of noble gases.

In this work, we explore the implications of the discovery of nebular Ne signatures on the formation history of the Earth and on the origin of its deep mantle noble gas reservoirs. We first construct in Section 2 an envelope formation model of Earth embryos embedded in the protoplanetary disk of the Sun based on the most recent planet formation models. We then connect the thermal state of forming primordial gas envelopes to the corresponding concentration of nebular gas dissolved in the mantle that would be measurable in deep mantle plumes. Section 3 presents our results, placing constraints on the properties of early Earth embryos. In Section 4, we discuss whether our results can be reconciled with the current understanding of the formation of the Earth, its interior reservoirs of other noble gases and its overall volatile budget. Finally, we summarize our findings in Section 5.

2. METHODS

In this section, we build a formation model of Earth embryos, self-consistently connecting the primordial solar system nebula to the observed nebular signatures of non-radiogenic ²²Ne in the Earth's deep mantle. We use the following nomenclature to describe the internal structure of Earth embryos, as depicted in Figure 1. The rocky interior consists of a silicate mantle that overlays an iron core, and the mantle + core structure accretes a surrounding gaseous envelope which we solve for with structure equations. As shown in Section 3, our calculations yield an atmosphere divided into a convective interior and a radiative exterior.³

We first develop in Section 2.1 a gas accretion calculation of primordial atmospheres atop Mars to Earth-sized

³ Hydrodynamical studies (M. Lambrechts & E. Lega 2017; A. Popovas et al. 2018; W. Béthune & R. R. Rafikov 2019; T. W. Moldenhauer et al. 2021; A. Bailey & Z. Zhu 2023) of envelopedisk interactions report an additional advective outer layer in the super-Earths/sub-Neptunes regime, within which recycling flows from the disk restrict the envelope to ~ 30% of its radius. Repeating the advection calculations of V. Savignac & E. J. Lee (2024), we find that atmospheric recycling can be ignored in this study of Earth embryos, since the additional advective layers rapidly cool, rendering them effectively indistinguishable from the otherwise near-isothermal radiative outer envelope.

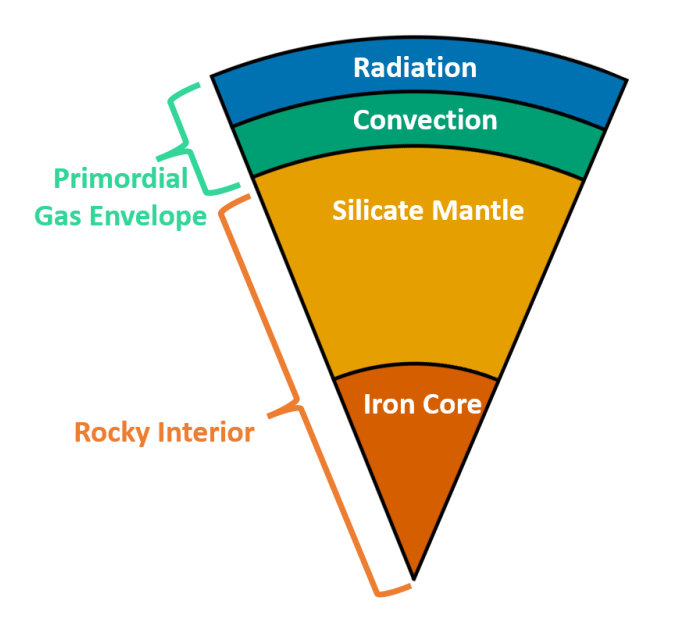


Figure 1. Layered structure of Earth embryos considered in this work. Embryos are divided into a rocky interior and a surrounding gas envelope accreted from the primordial nebula of the solar system. We assume that the rocky interior is made of an innermost iron core and an outer silicate mantle, analogous to the Earth's current internal structure. As argued in Section 2.1, the energy transport within the inner and outer atmospheric layers is set by convection and radiation, respectively, which follows from the Schwarzschild criterion. Note that the figure is not to scale. In reality, the envelope dominates the volume despite its small contribution to the total embryo mass.

rocky protocores embedded in the primordial nebula. We subsequently compute in Section 2.2 the dissolved concentration of nebular Ne in the silicate mantle, regulated by the thermal state of the mantle-envelope boundary. Only a selection of runs for rocky interior masses less than $0.5M_{\oplus}$ are presented in Section 3, as this subset of our simulations are the one yielding relevant results to the problem at hand.

Our calculations work under the assumptions that Earth embryos remain at fixed orbital distance during gas accretion and that dust grains do not contribute to nebular opacities. Both assumptions are valid in a late-stage gas-depleted (but not gas-empty) environment, which we confirm to be a preferred solution a posteriori, see Section 4.1.1. Potential opacity contributions from dust grains are discussed in Section 4.1.2. Lastly, our model is constructed such that embryos with equal interior volatile concentrations coalesce, preserving their composition from the initial to the final stage of the Earth's assembly (see Section 4.2).

2.1. Gas accretion model

Based on the widely accepted bottom-up core accretion scenario of J. B. Pollack et al. (1996), we implement one-dimensional quasi-hydrostatic gas accretion calculations to track the envelope mass growth of planetary embryos embedded in primordial disks of gas and dust. We adapt the model of E. J. Lee et al. (2014), initially built to characterize the gas accretion processes of super-Earths, to study smaller, gas-poor Earth embryos. As discussed in Footnote 3, adding an additional upper advective layer (V. Savignac & E. J. Lee 2024) makes no difference in this problem. Here, we summarize the key features of the calculation and highlight the adjustments made in this study; for complete details, readers are referred to E. J. Lee et al. (2014).

The process consists of building a series of hydrostatic "snapshots" of a primordial gas envelope of mass $M_{\rm env}$, accreted onto a rocky interior of mass $M_{\rm rock}$. Each of these snapshots is obtained by integrating the standard stellar structure equations,

$$\frac{dM(< r)}{dr} = 4\pi r^2 \rho,\tag{1}$$

$$\frac{dP}{dr} = -\frac{GM(< r)}{r^2}\rho - \frac{GM_{\odot}r}{a^3}\rho,\tag{2}$$

$$\frac{dT}{dr} = \frac{T}{P} \frac{dP}{dr} \nabla,\tag{3}$$

for the pressure P, density ρ , temperature T and enclosed mass $M(< r) \equiv M$ of the gas envelope as functions of the planetary radius r. Here, G is the gravitational constant, a is the fixed orbital distance and $\nabla \equiv d \ln T/d \ln P$ is the dimensionless temperature gradient of the primordial gas. As suggested by Z. Zhu et al. (2021), we account for the effect of the Sun's gravitational field on the hydrostatic balance of the envelope. The ensuing additional term in Equation (2) is effectively a minor correction, especially at a > 0.1 au around a solar mass star.

We assume the nebular composition to be solar (N. Grevesse & A. Noels 1993), with fixed values of $X=0.70,\,Y=0.28$ and Z=0.02 for the relative mass fractions of H, He and metals (i.e. elements heavier than H and He), respectively. Within the atmosphere, we implement the ideal equation of state (EOS) of E. J. Lee et al. (2014), which accounts for the different molecular, atomic, and ionized states of H as functions of temperature and pressure, as well as atomic He and metallic species at the aforementioned abundance rate.

The rate at which a forming planet accretes gas from the surrounding nebula is controlled by the thermal contraction of its gas envelope (e.g., J. B. Pollack et al. 1996; M. Ikoma et al. 2000; E. J. Lee et al. 2014; A.-M. A. Piso et al. 2015). We thus carefully make use of a realistic treatment of the cooling of the envelope with the gradient ∇ set by the dominant form of energy transport, either radiation

$$\nabla_{\rm rad} = \frac{3\kappa P}{64\pi G M \sigma_{\rm SB} T^4} L,\tag{4}$$

or convection

$$\nabla_{\rm ad} = -\frac{\partial \log S}{\partial \log P} \Big|_{T} \Big(\frac{\partial \log S}{\partial \log T} \Big|_{P} \Big)^{-1}. \tag{5}$$

Here, κ is opacity, $\sigma_{\rm SB}$ is the Stefan-Boltzmann constant, L is the luminosity of the envelope, and S is the specific entropy of the gas. We set $\nabla = \nabla_{\rm ad}$ when the Schwarzschild criterion is satisfied

$$\nabla_{\rm rad} > \nabla_{\rm ad},$$
 (6)

assuming no compositional gradients, and $\nabla = \nabla_{\rm rad}$ otherwise.

The opacity of the nebular gas has a significant effect on its cooling, and by extension gas accretion rates (M. Ikoma et al. 2000; E. J. Lee et al. 2014; A.-M. A. Piso et al. 2015). In late-stage protoplanetary disks such as the one in which primordial Earth embryos are presumed to accrete their atmosphere (see Section 4.1.1), dust grains are expected to have coagulated and rained out so that they no longer contribute to the opacity (C. Mordasini et al. 2014; C. W. Ormel 2014). We therefore adopt a "dust-free" opacity model based on the tabulated values of J. W. Ferguson et al. (2005) and R. S. Freedman et al. (2014). In the absence of dust grains, molecular opacities dominate at low temperatures below the H₂ dissociation front $(T \sim 2500 \text{K})$, and H⁻ opacities otherwise dominate the higher temperature regimes. Section 4.1.2 discusses the impact of potential opacity contributions for dust grains.

A major simplification of our calculation is the assumption that the envelope luminosity L is spatially invariant for each hydrostatic profile, which implicitly neglects the contribution of the outer radiative layers. This choice is justified by the centrally concentrated mass structure of the envelope due to H_2 dissociation driving the adiabatic index $\gamma < 4/3$, localizing the thermal inertia of the atmosphere to its inner convective layers. Following A.-M. A. Piso & A. N. Youdin (2014); E. J. Lee et al. (2014), we verify a posteriori the validity of this assumption by computing the neglected luminosity generated in the outer radiative envelope,

$$L_{\text{negl}} = -\int_{\text{rad}} \rho T \frac{\Delta S_M}{\Delta t} 4\pi r^2 dr. \tag{7}$$

Here ΔS_M is the difference of S evaluated at a given mass M between snapshots separated by a time Δt . We find that for dust-free envelopes at ~ 1 au, we can safely ignore $L_{\rm negl}$ since $L_{\rm negl}/L \lesssim 10\%$.

Consequently, each hydrostatic snapshot can be assigned a constant luminosity eigenvalue L that is solved for iteratively until the mass profile agrees with the fixed value of $M_{\rm env}$ within a relative difference of 1%. We construct snapshots for an increasing series of $M_{\rm env}$, which are then threaded in time by calculating the cooling time from one snapshot to the next. We ignore the thermal energy released from the rocky interior and return to the implications of this assumption in Section 4.5.

For the boundary condition, we adopt the fiducial minimum-mass solar nebula (MMSN) parameters for the gas density and temperature profiles of C. Hayashi (1981),

$$\rho_{\text{disk}} = 1.4 \times 10^{-9} \text{g cm}^{-3} \left(\frac{a}{1_{\text{BH}}}\right)^{-2.75} f_{\text{dep}},$$
 (8)

$$T_{\text{disk}} = 280 \text{K} \left(\frac{a}{1 \text{au}}\right)^{-1/2},\tag{9}$$

evaluated at a fixed orbital separation of a=1 au, where $f_{\rm dep} \leq 1$ is a gas depletion factor we vary, representing different evolutionary stages of nebular disks. We leave $f_{\rm dep}$ as a free parameter, constrain its possible values in Section 3, and discuss its relation to formation timescales in Section 4.1.

The state variables (P,T,ρ) smoothly transition from the outer nebular conditions to the envelope, and the differential system is integrated inward to the surface of the silicate mantle, at $R_{\rm rock} \equiv R_{\oplus} \left(\frac{M_{\rm rock}}{M_{\oplus}}\right)^{1/3}$ (D. Valencia et al. 2006). The outer boundary of the envelope is set by the Bondi radius, as appropriate for low mass sub-Earth embryos at 1 au

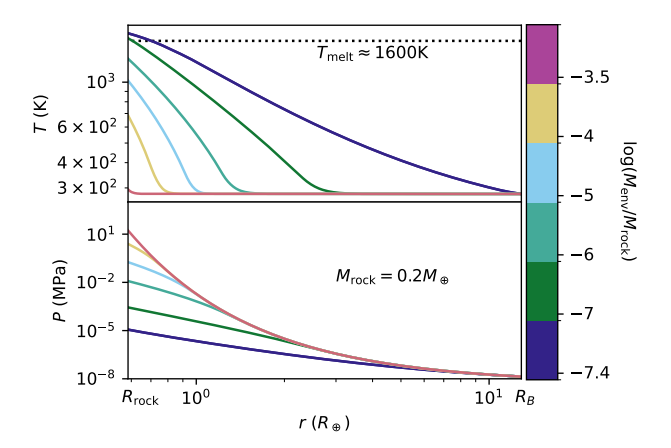
$$R_B = \frac{GM_p}{c_s^2} \simeq 64R_{\oplus} \left(\frac{M_p}{M_{\oplus}}\right) \left(\frac{\mu_{\text{disk}}}{2.37}\right) \left(\frac{a}{1 \text{ au}}\right)^{1/2}, \quad (10)$$

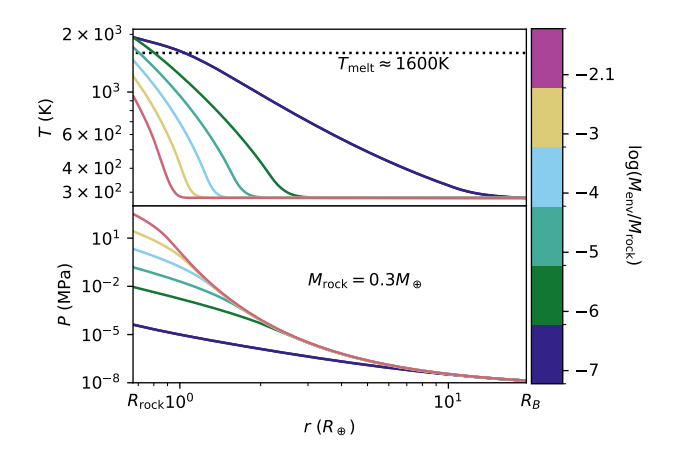
where $M_p \equiv M_{\text{rock}} + M_{\text{env}}$ is the total planetary mass, the sound speed

$$c_s = \sqrt{\frac{k_B T_{\text{disk}}}{\mu_{\text{disk}} m_{\text{H}}}} \tag{11}$$

is set by the disk temperature (Equation 9), the mean molecular weight of the MMSN disk ($\mu_{\rm disk} \approx 2.37$) is computed from the EOS, k_B is the Boltzmann constant and $m_{\rm H}$ the mass of the hydrogen atom.

Figure 2 shows examples of the envelope formation calculation for $M_{\rm rock}=0.2M_{\oplus}$ and $M_{\rm rock}=0.3M_{\oplus}$





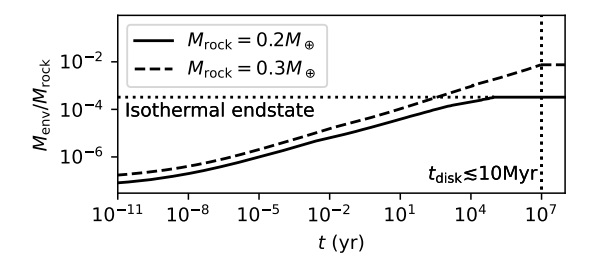


Figure 2. Formation of primordial gas envelopes atop rocky interiors embedded at 1 au in the minimum-mass solar nebula of C. Hayashi (1981), with gas density depleted by a factor of $f_{\text{dep}} = 10^{-2}$ (see Equation 8). Top: Radial profiles (solid) of the temperature and pressure (T, P) of the envelope with mass $M_{\rm env}$ for a rocky interior of mass $M_{\rm rock} = 0.2 M_{\oplus}$, extending from the radius of the rocky interior R_{rock} to the Bondi radius R_B . Each color represents a hydrostatic snapshot of the envelope for specific values of $M_{\rm env}/M_{\rm rock}$. The dotted line indicates the melting temperature $T_{\rm melt} \approx 1600 {\rm K}$ of the surface of the basaltic mantle (V. S. Solomatov & L. N. Moresi 2000). Center: Same as top, but for $M_{\text{rock}} = 0.3 M_{\oplus}$. Bottom: Time evolution of $M_{\rm env}/M_{\rm rock}$ for rocky interiors of mass $M_{\text{rock}} = 0.2 M_{\oplus}$ (solid) and $M_{\text{rock}} = 0.3 M_{\oplus}$ (dashed). The expected maximal disk lifetime (E. E. Mamajek 2009) is shown with a dotted vertical line. A horizontal dotted line denotes the isothermal endstate of the $M_{\rm rock} = 0.2 M_{\oplus}$ case.

Earth embryos accreting gas from a depleted nebula with $f_{\rm dep}=10^{-2}$. In both cases, the initially fully convective envelope cools, releasing its thermal energy in the disk as radiative near-isothermal layers begin to grow in the outer regions. Accretion is halted either when the envelope cools down to a near-isothermal end state (e.g., top panel of Figure 2) or when the gas disk with typical lifetimes of $\lesssim 10 {\rm Myr}$ (E. E. Mamajek 2009; R. Alexander et al. 2014; A. Michel et al. 2021) dissipates (e.g., middle panel of Figure 2).

2.2. Dissolution of primordial gas in the deep mantle

We develop a dissolution calculation under the assumption that a fraction of the total Ne budget of the primordial envelope is stored in the mantle during accretion, following equilibrium chemistry (i.e., balance of chemical potentials between dissolved and undissolved gas). From Henry's law, the primordial concentration $c_{22\text{Ne,p}}$ of nebular ^{22}Ne initially dissolved in the melt is

$$c_{^{22}\text{Ne,p}} = \frac{n_{^{22}\text{Ne}}P_0}{\mu^{M_{\text{Basalt}}}k_{\text{Ne}}}.$$
 (12)

Here, $n_{^{22}\mathrm{Ne}}$ is the elemental abundance of $^{22}\mathrm{Ne}$ in the solar nebular, $P_0 \equiv P(R_{\mathrm{rock}})$ is the surface pressure of the envelope-mantle boundary, $\mu^{M_{\mathrm{Basalt}}}$ is the molar mass of the molten silicate mantle and k_{Ne} is the Henry's Law constant of Ne in basaltic melts. We assume that different isotopes of an element share the same solubility constant, in the absence of evidence to the contrary.

For simplicity, we assume a fixed melting temperature for the formation of surface magma oceans of $T_{\rm melt} \approx 1600 {\rm K}$, typical for surface pressures on the order of $\sim 0.1 {\rm MPa}$ (V. S. Solomatov & L. N. Moresi 2000), and dissolution in the mantle is only allowed when the surface temperature $T_0 \equiv T(R_{\rm rock})$ is greater than this reference value.⁴ Based on thermodynamical models of phase relations in silicate melts (M. M. Hirschmann 2000; E. L. Tomlinson & T. J. B. Holland 2021), we find that the mantle solidus point exhibits only a weak dependence on pressure for $P_0 \lesssim 1$ GPa. This conclusion justifies our assumption of a pressure-independent melting point over the large range of surface pressures covered in our calculations ($\sim 10^{-3} - 10^3 {\rm MPa}$, see Figure 2).

We use a 22 Ne elemental abundance in the primordial nebula of $n_{^{22}\mathrm{Ne}}=(7.24\pm0.83)\times10^{-6}$ obtained

⁴ Here, the base temperature of the atmosphere $T(R_{\text{rock}})$ is presumed to smoothly transitioned to the surface temperature of the melt T_0 over the entire accretion process. In reality, the mantle thermally responds to changes in T_0 , over timescales discussed in Section 4.5.

via three-dimensional (3D) radiative-spectroscopic hydrodynamical analyses of the solar photosphere (see M. Asplund et al. 2021, their Table 2). In theory, the differential solubility of each atmospheric species, mainly that of H and He which dominate the primordial gas (see Sections 4.3-4.4), along with rapid mixing timescales in the deep convective envelope could alter atmospheric composition. We verify a posteriori that the mass of volatiles infused in the mantle throughout the entire accretion process is small compared to the total atmospheric budget for H ($\lesssim 3\%$), He ($\lesssim 3\%$), and metals $(\leq 0.1\%)$. Subsequent changes in the atmospheric composition can therefore be ignored with small fractional changes of $\Delta X/X \approx \Delta Y/Y \lesssim 0.06\%$ and $\Delta Z/Z \lesssim 3\%$. This verification validates the assumption of a constant envelope chemical composition and simplifies the dissolution calculation.

Regarding the solubility constant, G. Iacono-Marziano et al. (2010) characterized the linearity of the solubility of He, Ne and Ar with pressure in silicate melts, in agreement with the previous work of A. Jambon et al. (1986). From the basaltic lava samples of the 2002 Mt. Etna eruption with $\mu^{M_{\text{Basalt}}} = 64.13 \pm 0.38 \text{mol/g}$ (see their Table 1), G. Iacono-Marziano et al. (2010) developed a model to compute the solubility constant of Ne (along with He and Ar) within 22% of uncertainty as a function of temperature and pressure, representative of the behavior of gas in basaltic melt up to 3 GPa and 1600 °C. We use their provided worksheet (see their supplementary data) to compute k_{Ne} as a function of T_0 and P_0 . In lack of complementary calculations for higher temperatures $(T_0 \gtrsim 1600\text{C} = 1873.15\text{K})$, we extrapolate the solubility model of G. Iacono-Marziano et al. (2010) using their Equations (8-10) to the higher values of $T_0 \lesssim 2500$ K retrieved at the bottom of our computed primordial envelopes (see Figure 2).

After formation over ~ 4.5 Gyr of evolution of the Earth, the dissolved gas can be outgassed by the continuous motion of tectonic plates, mantle convection, and volcanic activity, which are expected to drive a steady outgassing rate of volatiles from the mantle (J. Lupton & H. Craig 1975; K. Farley et al. 1995; M. L. Bender et al. 2008; D. Bianchi et al. 2010; M. Moreira 2013). To account for these effects, we adopt the best-fit forward model of R. Parai (2022) to calculate the fraction of the noble gas content of the mantle that was lost due to outgassing. They argued that even though the lower mantle

has been more efficient at retaining its initial gas than the upper mantle, it still suffered significant degassing. From their best-fit parameters (see their Figure S6) for the plume mantle, we find that the initial deep mantle Ne reservoir was ≈ 18.7 times more enriched relative to the present-day budget. We consequently multiply the quoted concentration of the deep mantle ²²Ne reservoir (B. Marty 2012; A. N. Halliday 2013) by ≈ 18.7 to correct for mantle outgassing in Section 3.

3. RESULTS

With the one-dimensional differential system presented in Section 2.1, we simulate the envelope growth of planetary embryos ranging from $M_{\rm rock}=0.1M_{\oplus}$ to $M_{\rm rock}=0.5M_{\oplus}$. We do not consider embryos of higher masses because of the evidence of the Earth's formation via giant impact(s) post-nebular dispersion (J. M. Tucker & S. Mukhopadhyay 2014), which requires protoplanets of mass $M_{\rm rock}\leq 0.5M_{\oplus}$. We explore depletion factors of $\log f_{\rm dep}\in[0,-1,-2,-3,-4]$ (see Equation 8) to explore formation at later stages of the lifetime of the disk, as the latter gradually dissipates.

We find that dissolution of nebular gas is only possible in the early stages of envelope formation, as the surface temperature of the envelope-mantle boundary quickly reaches the solidification temperature of the mantle (i.e. $T_0 \approx T_{\rm melt}$). We therefore stress the importance of adopting a careful treatment of the cooling of primordial envelopes to avoid overestimating the dissolved concentration of noble gases in the mantle. For example, if one were to calculate the dissolved fraction of $^{22}{\rm Ne}$ in the mantle (using Equation 12) based on the nearisothermal end state of the envelope shown in the top panel of Figure 2, the primordial Ne budget of the mantle would be overestimated by several orders of magnitude due to the large increase of P_0 from $\approx 10^{-5}$ MPa to ≈ 10 MPa during the gas accretion stage.

Our gas accretion calculation also argues that the dissolution timescale of volatiles required to reach the $^{22}\mathrm{Ne}$ target concentration in the deep mantle is very short ($\lesssim 10^{-2}\mathrm{yr}$, see Figure 2). We therefore cannot use this model to establish clear constraints on the formation timescales of primordial envelopes in the disk or on the lifetime of the nebula itself. For example, embryos accreting gas from a disk with $f_{\rm dep}=10^{-2}$ on any timescale $\Delta t\gtrsim 10^{-2}$ yr on top of a $0.3M_{\oplus}$ core would contain similar dissolved concentrations of $^{22}\mathrm{Ne}$ in their mantle.

Following the procedure of Section 2.2, we calculate the concentration $c_{^{22}\mathrm{Ne,p}}$ of primordial $^{22}\mathrm{Ne}$ dissolved in the mantle at surface pressure P_0 in the presence of magma oceans $(T \geq 1600\mathrm{K})$ during early accre-

 $^{^5}$ For reference, the behavior of the solubility constant is well approximated by $k_{\rm Ne} \approx (1.11 \pm 0.24) \times 10^5 {\rm MPa} \Big(\frac{T_0}{1600 {\rm K}}\Big)^{-1.762}$ over the surface temperature and pressure ranges covered in our calculations.

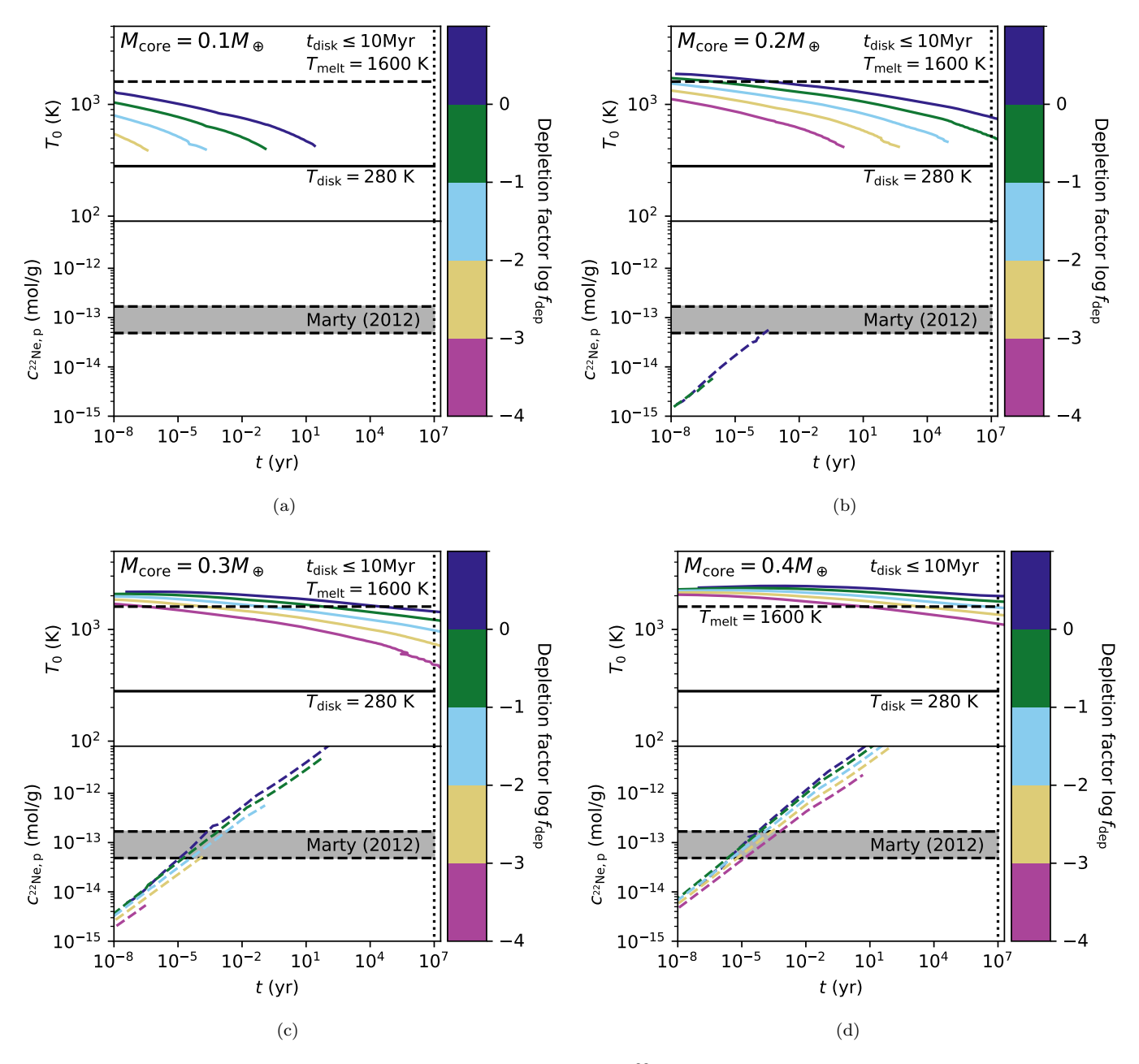


Figure 3. Dissolution calculation of the concentration of primordial 22 Ne captured at the molten surface of magma oceans on Earth embryos embedded in the solar nebula. Subfigures (a), (b), (c) and (d) present our results for protocore masses of $0.1, 0.2, 0.3, 0.4M_{\oplus}$, respectively. For each case, the upper panel shows the temperature T_0 of the envelope-mantle boundary as a function of time and the lower panel the resulting concentration of primordial 22 Ne dissolved in the silicate interior $c_{22}_{\text{Ne,p}}$ before the surface of the mantle solidifies at a melting temperature $T_{\text{melt}} \approx 1600\text{K}$ (V. S. Solomatov & L. N. Moresi 2000). The shaded areas represent the target concentration required to explain the present-day budget of the deep mantle, as constrained by B. Marty (2012) and corrected by a factor of ≈ 18.7 to account for mantle outgassing (R. Parai 2022). The solid black line indicates the temperature T_{disk} of the minimum-mass solar nebula (MMSN) of C. Hayashi (1981) and the black dashed line the melting temperature T_{melt} of the basaltic mantle (V. S. Solomatov & L. N. Moresi 2000), required at the surface for the dissolution of primordial gas in the interior. The upper bound on the lifetime of the disk (E. E. Mamajek 2009) is indicated with a dotted vertical line, corresponding to the maximal possible time after which primordial accretion must come to an end. Different colors account for different depletion factors $f_{\text{dep}} \leq 1$ of the gas density of the MMSN disk.

tion. Figure 3 presents our findings for embryo mass of $M_{\text{rock}} = [0.1, 0.2, 0.3, 0.4] M_{\oplus}$.

We find that protocores of mass $\lesssim 0.1 M_{\oplus}$ do not exhibit the high surface temperatures required for the existence of magma oceans. Due to their limited mass, these bodies generate less accretional heat and cool more efficiently, and their surface temperature T_0 never exceeds the solidification point of the basaltic melt. The evidence of nebular reservoirs in the mantle therefore places a lower bound of $\sim 0.2 M_{\oplus}$ on the mass of the ancestors of the Earth that accreted primordial nebular gas.

For larger embryos with surface temperatures that allow envelope-mantle mixing, we aim to compare our predicted Ne reservoirs with the present-day budget of the deep mantle, correcting for mantle outgassing. Using a global mass balance analysis of the Earth's inventory of ⁴⁰Ar, B. Marty (2012) derived the volatile composition of the bulk silicate mantle (i.e. the non-degassed mantle) and constrained its concentration of ²²Ne to $c_{^{22}\text{Ne,DM}} = (5.8 \pm 3.2) \times 10^{-15} \text{mol/g}$. We adopt this concentration for deep mantle reservoirs, but also note that similar calculations by A. N. Halliday (2013) predict a lower Ne budget by $\approx 1\sigma$, with the discrepancy arising from the uncertainty in extrapolating the compositions of OIB samples to the deep inner mantle. Guided by the results of C. D. Williams & S. Mukhopadhyay (2019), we assume for simplicity that this entire Ne reservoir in the deep mantle is of nebular origin. This corresponds, after accounting for mantle degassing, to an initial concentration of $c_{^{22}\text{Ne,p}} = (1.08 \pm 0.60) \times 10^{-13} \text{mol/g}$ dissolved during the accretion of a primordial envelope, which we set to our target value. Secondary contributions from accreted chondrites and/or subducted atmospheric gas are expected to be minor ($\lesssim 10-15\%$) (S. Peron & S. Mukhopadhyay 2022), and are discussed in Section 4.3.

Comparing with the reference from B. Marty (2012) in Figure 3, we first find that the nebular Ne reservoir can be explained (albeit just barely) by accretion within early, gas-rich ($f_{\rm dep} = 1$), MMSN disks onto $\sim 0.2 M_{\oplus}$ Earth embryos. However, in depleted $(f_{\rm dep} \lesssim 10^{-1})$ density environments, the mantle of $\sim 0.2 M_{\oplus}$ embryos solidifies too quickly to reach an agreement with the measurements of B. Marty (2012). A late stage formation scenario (E. J. Lee & E. Chiang 2016) of rocky protocores in the disk, typically corresponding to depleted $(f_{\rm dep} \lesssim 10^{-2})$ protoplanetary disks, would instead require protocores of mass $M_{\rm rock} \sim 0.3 M_{\oplus}$, above which an excess of noble gases would be injected in the rocky interior. For both the $M_{\rm rock} \sim 0.2 M_{\oplus}$ and the $M_{\rm rock} \sim 0.3 M_{\oplus}$ solutions, the dissolution timescale required to reach the $c_{^{22}\text{Ne,p}} = (1.08 \pm 0.60) \times 10^{-13} \text{mol/g}$ target is very short ($\lesssim 0.01 \text{ yr}$) and justifies the use of a time-independent disk profile (Equation 8), since the disk gas density would not evolve substantially over this short time frame.

We discuss in Section 4.2 how a surplus of dissolved volatile content in the deep mantle post-accretion is unlikely to be ejected via subsequent mass loss events such as giant impacts. Consequently, the accretion of a primordial envelope $\gtrsim 0.4 M_{\oplus}$ protocores, which would dissolve $\gtrsim 10$ times the expected ²²Ne concentration, would be inconsistent with the current Ne budget of the deep mantle. This conclusion establishes an upper limit on the mass of Earth embryos that must have formed in the solar nebula.

In summary, our model argues that protocores of masses $M_{\rm rock} \sim 0.2-0.3 M_{\oplus}$ must have formed and accreted a gas envelope from the nebula, rapidly dissolving the measured primordial ²²Ne concentration in the deep mantle. Given the quick drop in the required disk density from $f_{\rm dep}=1$ for the marginal case of $0.2 M_{\oplus}$ embryos to $f_{\rm dep} \sim 10^{-2}-10^{-3}$ for the $M_{\rm rock}=0.3 M_{\oplus}$ solution, we conclude that Earth embryos most likely formed in the late-stage depleted nebula (see Section 4.1). These results are in agreement with the analogous study of the imprint of a nebular atmosphere on the interior of Mars-mass embryos of E. Jaupart et al. (2017). They established a similar lower bound of $M_{\rm rock} \sim 0.2 M_{\oplus}$ on the planetary embryo mass required to capture the present-day Ne contents of the Earth's mantle.

4. DISCUSSION

4.1. Embryo formation in the primordial nebula

We have so far worked under the assumption that fully assembled Earth embryos accreted their primordial gas envelope in-situ at a=1 au in the later stages of the solar nebula, at a time when dust grains no longer contributed to the opacity. This choice allows us to present a self-consistent solution for which $\sim 0.3 M_{\oplus}$ embryos build their envelope in the gas-poor ($f_{\rm dep} \sim 10^{-3} - 10^{-2}$) environment of the nebula near its dispersal. Here, we assess the validity of this primary assumption and investigate how departures from it may impact our results.

4.1.1. Consistent formation scenario in a late-stage nebula

Solid growth of Earth embryos can proceed through planetesimal accretion (V. S. Safronov & E. V. Zvjagina 1969; V. S. Safronov 1972; C. Hayashi et al. 1985; G. W. Wetherill & G. R. Stewart 1989; S. Ida & J. Makino 1993), where km-scale bodies collide and merge, and/or through pebble accretion (C. W. Ormel & H. H. Klahr 2010; A. Johansen & P. Lacerda 2010), where mm-cm sized particles drifting inward via aerodynamic drag in

the disk are efficiently captured by individual accretors. Since there remains debate as to which of these accretion mechanisms predominantly drives embryo formation in the early solar system (A. Izidoro et al. 2021; I. J. Onyett et al. 2023; A. Morbidelli et al. 2025), we remain agnostic to the specific pathway by which Earth embryos were assembled.

That said, it must be noted that both scenarios, along with the possibility of mergers via early giant impacts, can easily lead to the formation of $0.2-0.3M_{\oplus}$ Earth embryos at ~ 1 au in the solar nebula within 1-5 Myr (S. J. Weidenschilling et al. 1997; E. Kokubo & S. Ida 2000; J. Chambers 2006; K. J. Walsh & H. F. Levison 2016; K. J. Walsh & H. F. Levison 2019; A. Izidoro et al. 2021; A. Johansen et al. 2021). Furthermore, migration in low density protoplanetary disks is expected to be inefficient for $\sim 0.1-0.5M_{\oplus}$ proto-planets due to the limited torque from the gas (H. Tanaka et al. 2002). Most formation models of the inner solar system suggest that the terrestrial planets formed largely in-situ, while the giant planets experienced the bulk of migration (B. M. S. Hansen 2009; S. A. Jacobson & A. Morbidelli 2014; N. A. Kaib & J. E. Chambers 2016; R. Brasser 2025; A. Morbidelli et al. 2025). It is therefore fairly reasonable to consider the formation of $\sim 0.3 M_{\oplus}$ ancestors of the Earth near ~ 1 au within the first few Myr of the solar system.

The remaining key question to be answered is the state of the solar nebula at the time those embryos emerged, which is challenging to determine. Observationally, the lifetime of protoplanetary disks around Sun-like stars has been inferred to be 1-10 Myr (E. E. Mamajek 2009; R. Alexander et al. 2014; A. Michel et al. 2021) from observations of young stellar objects. For the Sun, modern formation models of the gas giants (e.g., O. G. Benvenuto et al. 2009; G. D'Angelo et al. 2021) and the solar system as whole (e.g., the Grand Tack model of K. J. Walsh et al. 2011) require the presence of the gaseous nebula up to ~ 3 Myr into the formation of the solar system.

Although remnants of the primordial nebula in the Earth's deep mantle do not directly constrain the disk dissipation timescale, our results argue that the emergence of $\sim 0.3 M_{\oplus}$ Earth embryos must have coincided with the dispersal of the gas disk. Indeed, primordial gas must be present, but not too much $(10^{-4} \lesssim f_{\rm dep} \lesssim 10^{-2})$ to explain the concentration of primordial gas in the rocky interior of embryos.

The formation of primordial atmospheres in a gaspoor nebula is consistent with our use of dust-free opacity grids. As the disk evolves on \sim Myr timescales, solid dust grains in the disk either grow into bigger objects (e.g., pebbles, planetesimals, embryos, C. W. Ormel 2014; C. Mordasini et al. 2014), drift radially inward toward the Sun (G. Laibe et al. 2012), or are blown out via photoevaporation and disk winds (P. J. Rodenkirch & C. P. Dullemond 2022). Even more so, dust grains within primordial atmospheres can settle ("rain out") toward deeper layers, thereby favoring dust-free regimes (C. W. Ormel 2014; C. Mordasini 2014). In the absence of the opacity contribution of dust grains, thin primordial envelopes are rapidly accreted as they efficiently cool, quickly delivering volatiles to the rocky interior before mantle solidification.

4.1.2. Marginal solution in a gas-rich nebula

It must be noted that a marginal alternative scenario of $\sim 0.2 M_{\oplus}$ embryos forming in a gas-rich ($f_{\rm dep}=1$ disk remains plausible (see Figure 3(b)) and merits consideration. This is at odds with our dust-free opacity assumption, as we may expect disk opacities to gradually transition from "dusty" to dust-free regimes as the nebula dissipates. To evaluate the validity of this result, we repeated the gas accretion calculation of Section 2.1 with the dusty opacity grids of J. W. Ferguson et al. (2005), which assume an interstellar medium size distribution of dust grains.⁶

We find that the thermal (P,T) structure of individual snapshots is largely unaffected by the change in opacity grid, resulting in no significant variations in the dissolved ²²Ne concentrations reported in Figure 3. As the radiative outer layer extends inward, the dusty and dustfree envelopes transition to the deep layers following the same inner adiabat, resulting in similar P_0 values.

Unfortunately, the behavior of $\kappa(r)$ in dusty envelopes is non-monotonic, arising from significant opacity drops due to the sublimation of different grain species for $1500 \, \mathrm{K} \lesssim T \lesssim 2500 \, \mathrm{K}$. This complex opacity profile leads to deviations from the simple envelope structure (innermost convective + outer radiative layers) of dust-free envelopes presented in Figure 2, with additional inner and intermediary radiative shells. As such, the major assumption in our gas accretion model of a spatially constant luminosity fails for dusty envelopes, with large neglected contributions from inner radiative layers in Equation (7) (i.e. $L_{\mathrm{negl}} \gtrsim L$). We therefore cannot use our scheme to resolve the precise time evolution of primordial dusty envelopes, as is done for dust-free regimes in Figure 2.

The timescale required to dissolve the required ²²Ne in a dusty environment can nonetheless be estimated

⁶ The J. W. Ferguson et al. (2005) opacity table cuts off below $T=500\mathrm{K}$, where we extrapolate using a $\kappa \propto T^2$ scaling.

by comparing the thermal structures between dusty and dusty-free envelopes. As illustrated in Figure 2, the thin primordial envelopes accreted by small embryos lie in a temperature regime ($T \lesssim 2500 \mathrm{K}$) where H⁻ ions do not dominate the opacity. When present, dust grains therefore control the opacity, with dusty values being roughly three orders of magnitude higher than molecular opacities. In more opaque environments, planetary envelopes cool at a linearly slower rate since $L \propto \frac{1}{\kappa}$ (see Equation 4). The formation of the primordial envelope and the subsequent transport of volatiles to the mantle thus progress more slowly, stretching the timescale of our marginal solution of $0.2 M_{\oplus}$ rocky interiors (see Figure 3(b)) from only 3 hours for a dust-free envelope to ~ 125 days for a dusty equivalent.

Overall, the presence of dust grains in the early nebular gas would not alter the concentrations displayed in Figure 3, but only slow the accretion and dissolution processes. Consequently, the marginal solution of Figure 3(b) for which $\sim 0.2 M_{\oplus}$ embryos form in an early gas-rich disk with dusty opacities cannot be ruled out.

4.2. Final assembly of the Earth

Thus far we have focused on the assembly of $\leq 0.4 M_{\oplus}$ planetary embryos in the solar nebula. It is widely understood that the final coalescence of the Earth occurred via giant impacts (M. Meier et al. 2014), where like-sized proto-planets collide and merge (e.g., C. B. Agnor et al. 1999). This section links the formation of Earth embryos to the planet's present state and provides a unified picture of its evolution in Figure 4.

4.2.1. Evidence of giant impacts

According to the Giant Impact Hypothesis (W. K. Hartmann & D. R. Davis 1975; A. G. W. Cameron & W. R. Ward 1976), the formation of the final Earth-Moon system stems from a catastrophic collision of a young "proto-Earth" with a lower-mass protoplanet often referred to as "Theia" (A. N. Halliday 2000; B. L. Quarles & J. J. Lissauer 2015; N. A. Kaib & N. B. Cowan 2015). Evidence supporting this theory includes the spin and orbital properties of the Earth-Moon system being consistent with a massive collision (R. M. Canup 2008), the volatile depletion of the Moon implying high-temperature processing of the ejected material (J. M. D. Day & F. Moynier 2014), and the isotopic similarities between the Earth and the Moon (U. Wiechert et al. 2001). Converging lines of reasoning date this final assembly to $\sim 30-100$ Myr after the formation of Calcium-Aluminum-rich Inclusions (CAIs),⁷ using isotopic measurements in meteorites as chronometers (T. Kleine et al. 2009; J. F. Rudge et al. 2010), isotopic analyses of the Earth and the Moon (A. N. Halliday 2008), and dynamical models of their formation (C. B. Agnor et al. 1999; S. N. Raymond et al. 2009).

Details of the proto-Earth-Theia collision have been investigated by many studies (e.g. R. M. Canup 2004; M. Ćuk & S. T. Stewart 2012; R. M. Canup 2012). The original idea of a "Moon-forming" impact describes a collision between a proto-Earth of mass $M_{\rm PE}\approx 0.9 M_{\oplus}$ and a Mars-sized Theia of mass $M_{\rm Theia}\approx 0.1 M_{\oplus}$ (W. K. Hartmann & D. R. Davis 1975; A. G. W. Cameron & W. R. Ward 1976; R. M. Canup 2004). In the classical scenario with an impactor-to-target mass ratio of $\phi\equiv M_{\rm Theia}/M_{\rm PE}\approx 1/9$, the Moon forms from an orbiting silicate disk primarily originating from the impactor's mantle, while the Earth's composition remains consistent with the original proto-Earth (R. M. Canup & E. Asphaug 2001).

This classical picture expects distinct compositions between the Earth and the Moon, but is challenged by their isotopic similarities in oxygen (U. Wiechert et al. 2001), chromium (G. Lugmair & A. Shukolyukov 1998), titanium (J. Zhang et al. 2012) and tungsten (N. Dauphas 2017; T. S. Kruijer & T. Kleine 2017). Invoking the coalescence of the proto-Earth and Theia in the same local disk environment to resolve this issue is difficult, as there is no guarantee that they would emerge with the same isotopic nature. Instead, R. M. Canup (2012) demonstrated that a larger impactor-totarget mass ratio of $\phi \approx 0.4 - 0.5$ allows more mixing between the proto-Earth and Theia, with the impactor contributing equally to the planet and disk produced from the collision. Such a merger of a $\sim 0.6-0.7$ proto-Earth and a $\sim 0.3 M_{\oplus}$ Theia would still satisfy the angular momentum constraint of the Earth-Moon system (M. Ćuk & S. T. Stewart 2012). An even higher Theia mass of $\sim 0.4 M_{\oplus}$ has been proposed by S. J. Desch & K. L. Robinson (2019) to explain the preservation of the Moon's water during the impact.

Moreover, comparisons of ${}^{3}\text{He}/{}^{22}\text{Ne}$ ratios between the upper degassed and lower preserved mantles suggest that an additional giant impact must have shaped the Earth's current internal structure. Giant impacts are capable of re-melting much of the Earth's mantle, re-creating global magma oceans and enabling the formation of secondary atmospheres via mantle outgassing

⁷ In this work, we do not distinguish between the onset of the solar system formation and the formation of CAIs, which are its earliest solids, and adopt this time as t=0.

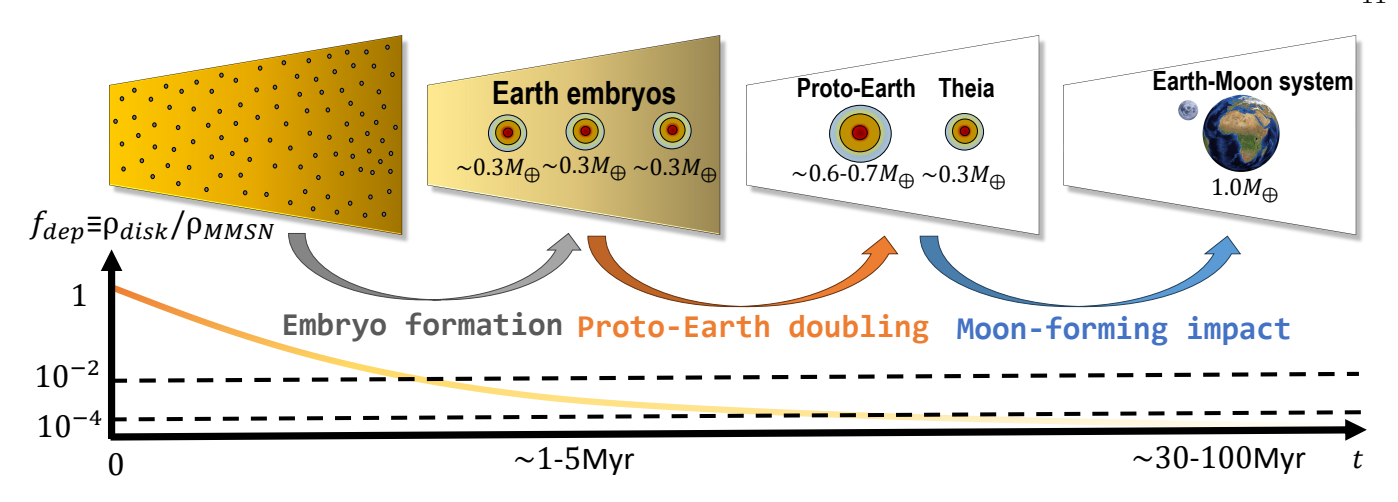


Figure 4. Schematic illustration of the favored Earth formation scenario implied by our results. Top: From left to right, we show the different formation stages of the Earth from a side-view of a truncated solar nebula, which is initially rich in gas (yellow) and dust (gray dots). As the disk progressively dissipates, the coagulation of solids (see Section 4.1.1) leads to the formation of a set of three $\sim 0.3 M_{\oplus}$ embryos, displayed with cyan, orange and red circles representing the layered embryo structure of Figure 1. Following the dispersal of the disk, embryo mergers are enabled, resulting in the formation of the proto-Earth via the doubling (orange arrow) of two $\sim 0.3 M_{\oplus}$ embryos. The proto-Earth later collides (blue arrow) with the remaining embryo (i.e. Theia) to form the final Earth-Moon system. Bottom: Time evolution (yellow curve) of the volume gas density $\rho_{\rm disk}$ of the solar nebula beginning from a full minimum-mass solar nebula density $\rho_{\rm MMSN}$, as parametrized by the parameter $f_{\rm dep}$ of Equation (8). Key values of $f_{\rm dep}=10^{-2}$ and $f_{\rm dep}=10^{-4}$ setting the boundaries between the gas-rich, gas-poor and dispersed stages of the disk are shown with dash horizontal lines.

(L. T. Elkins-Tanton 2012). Each outgassing/ingassing cycle increases $^3{\rm He}/^{22}{\rm Ne}$ values in the mantle, since He is preferentially dissolved in basaltic melts compared to Ne (A. Jambon et al. 1986; G. Iacono-Marziano et al. 2010). Consequently, J. M. Tucker & S. Mukhopadhyay (2014) established that one giant impact alone, even in the most drastic scenario, cannot raise the initial value of $^3{\rm He}/^{22}{\rm Ne}\sim 2.3-3$ for the more primitive deep mantle to the values of ≥ 10 reported for the depleted upper mantle. Instead, multiple magma ocean events are required, corresponding to at least two giant impacts.

4.2.2. A cohesive Earth formation pathway

In light of the current constraints on the final assembly of the Earth, we propose in Figure 4 a cohesive pathway to assemble the Earth, beginning with the emergence of a set of three $\sim 0.3 M_{\oplus}$ embryos in the late stages of the solar nebula. As discussed in Section 4.1.1, there is limited flexibility to envision alternative initial configurations of Earth embryos due to the tight constraints on the critical embryo mass of $\sim 0.3 M_{\oplus}$ in the later phases of the solar nebula.

In this scenario, the three Earth ancestors complete their assembly in the same local (\sim 1 au) environment of the depleted ($f_{\rm dep} \sim 10^{-4}-10^{-2}$) gas disk. At this time, they each rapidly accrete a primordial envelope and deliver the required concentration of primordial ²²Ne of $c_{\rm ^{22}Ne,p} \approx (1.08 \pm 0.60) \times 10^{-13} \rm mol/g$ as demonstrated by Figure 3(c). In the presence of the background neb-

ula, gas damping effectively circularizes embryo orbits, hindering further embryo growth via giant impacts until disk dispersal. Once the nebula dissipates, the damping of embryos' eccentricities e is effectively removed, enhancing the likelihood of their orbits crossing and triggering giant impacts.

We therefore propose the existence of an intermediary phase (third stage depicted in Figure 4), following nebular dispersal $(t \sim 1-5 \text{Myr})$ but prior to the Moonforming impact ($t \sim 30-100 \text{Myr}$), during which a young $\sim 0.6-0.7 M_{\oplus}$ proto-Earth coexisted in the vicinity of the remaining $\sim 0.3 M_{\oplus}$ embryo. In this context, the latter would correspond to the hypothesized ancient planet Theia, with a comparable size to the proto-Earth, as allowed by current terrestrial and lunar chemical constraints (Section 4.2.1). We favor a local formation of Theia as it is expected to have a similar composition to the proto-Earth (A. Mastrobuono-Battisti et al. 2015; N. Dauphas 2017). Subsequently, the final Earth-Moon system would be reached through the Moon-forming impact (blue arrow in Figure 4) between the proto-Earth and Theia.

Quantitatively, the feasibility of the proposed scenario of Figure 4 can be established by comparing the orbit-crossing timescale t_X of the embryos of mass m with their eccentricity damping timescales $t_{\rm damp} \equiv \frac{e}{\hat{e}}$. J. C. B. Papaloizou & J. D. Larwood (2000) established a criterion of $t_X < 10t_{\rm damp}$ to assess whether a given protoplanetary disk would favor embryo mergers, based

on their N-body dynamical simulations of agglomeration of protoplanetary cores. As derived by J. Binney & S. Tremaine (2008), the eccentricity damping timescale can be expressed as

$$t_{\rm damp} \sim \frac{c_{\rm s}^3}{G^2 m \rho_{\rm disk}} \sim 816 {\rm yr} \frac{M_{\oplus}}{m} \frac{1}{f_{\rm dep}},$$
 (13)

where c_s is evaluated in the MMSN disk at 1 au using Equations (9) and (11) and ρ_{disk} with Equation (8).⁸ Comparatively, J.-L. Zhou et al. (2007) developed an empirical formula for the orbit crossing timescale of the doubling of embryos of mass $m \to 2m$.

$$t_X(m, e, k) = 10^{A(m, e, k) + B(m, e, k) \log_{10}(k/2.3)} \text{yr}.$$
 (14)

Here, $k \equiv \Delta a/R_{\rm mH}$ is the orbital separations Δa of the objects in units of their mutual Hill radii

$$R_{\rm mH} = \left(\frac{2m}{3M_{\odot}}\right)^{1/3} a = 0.0126 \left(\frac{m}{M_{\oplus}}\right)^{1/3} a.$$
 (15)

The parameters

$$A = -2 + e/h - 0.27 \log_{10} \left(\frac{m}{M_{\odot}}\right) \tag{16}$$

and

$$B = 18.7 - 16.8e/h + (1.1 - 1.2e/h)\log_{10}\left(\frac{m}{M_{\odot}}\right) (17)$$

are fitted constants, where

$$h = \frac{k}{2} \left(\frac{2m}{3M_{\odot}}\right)^{1/3}.$$
 (18)

In Figure 5, we compute t_X for a range of possible orbital separations between the $0.3M_{\oplus}$ embryos of Figure 4, and compare it with $t_{\rm damp}$ in the depleted gas nebula. We fix e=0.001, as embryo eccentricities are expected to be small ($e\lesssim0.01$) for such high mass embryos in the later phase of the life of protoplanetary disks (S. Ida & D. N. C. Lin 2004). Consistently with the $M_{\rm rock}\sim0.3M_{\oplus}$ solution of Figure 3(c) with $10^{-4}\lesssim f_{\rm dep}\lesssim10^{-2}$, we find that a "proto-Earth doubling" merger of two $0.3M_{\oplus}$ embryos (denoted by an orange arrow in Figure 4) would have been facilitated (i.e. $t_X<10t_{\rm damp}$) by the dispersal of the gas

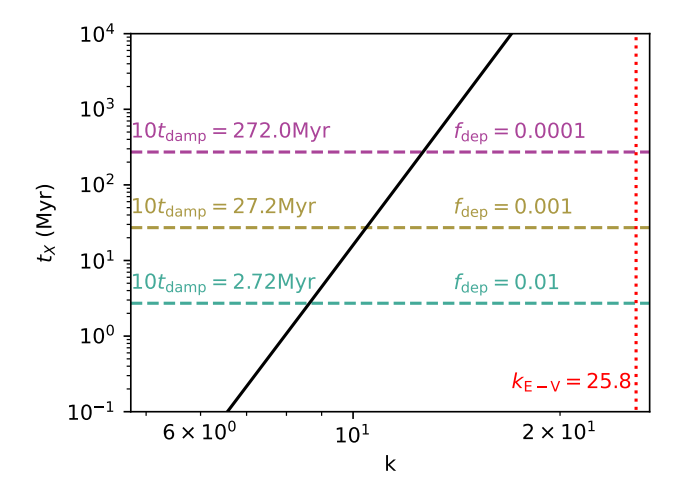


Figure 5. Orbit crossing time t_X of $0.3M_{\oplus}$ embryos assembled at $a \sim 1$ au with eccentricity e = 0.001, as a function of orbital spacing k. The eccentricity damping timescale $t_{\rm damp}$ of the embryos in a gaseous nebular depleted by factors $f_{\rm dep} = [10^{-2}, 10^{-3}, 10^{-4}]$ are displayed with cyan, yellow and magenta dashed horizontal lines, respectively. The damping times are multiplied by 10 to assess the merger criterion $t_X < 10t_{\rm damp}$ of J. C. B. Papaloizou & J. D. Larwood (2000). As a reference, the orbital spacing $k_{\rm E-V}$ between the Earth and its nearest neighbor Venus is indicated with a red dotted vertical line.

disk $(f_{\rm dep} \lesssim 10^{-3})$, with the orbits of embryos with $k \lesssim 10$ crossing within 30 Myr. Furthermore, eccentricity damping halts the mergers of $\sim 0.3 M_{\oplus}$ embryos in gas-rich $(f_{\rm dep} \gtrsim 10^{-2})$ for spacings $k \gtrsim 10$, explaining why the initial oligarchic growth of embryos (denoted with a gray arrow in Figure 4) would favor the critical embryo mass in the nebula. It is therefore reasonable to consider a first proto-Earth merger at $a \sim 1$ au of Earth embryos before the Moon-forming impact at $t \sim 30-100$ Myr, with an initial mean spacing between the embryos of $k \sim 10$, corresponding to orbital separations of $\Delta a \sim 0.08$ au.

We note that an initial embryo spacing of $k \sim 10$ for the entire inner solar system would be inconsistent with the current Earth-Mars spacing of $k_{\rm E-M}=39.9$, but would marginally agree with the spacing of $k_{\rm E-V}=25.8$ between the Earth and Venus. Indeed, each global embryo doubling event $(m \to 2m)$ increases the average value of k in a system by a factor of $2^{2/3} \approx 1.6$ (by definition of k and Equation 15). As such, a set of Venus, Earth and Mars embryos emerging from early assembly in the nebula with mean spacings $k \sim 10$ would lead to average spacings of $k \sim 25$ after two doubling events. The discrepancy with the Earth-Mars spacing may be a result of Mars not participating in later growth phases, consistent with the evidence of Mars being a

⁸ For simplicity, the velocity of embryos relative to the gas is assumed to be $\sim c_s$, dominated by their eccentric and headwind motion, which is subsonic. This approximation is valid for embryos with eccentricities $e \lesssim c_s/v_K \sim 1/30$, where $c_s \sim 10^5 {\rm cm/s}$ (Equation 11) and the Keplerian velocity $v_K \sim 3 \times 10^6 {\rm cm/s}$ is evaluated at 1 au.

stranded planetary embryo formed early in the nebula (N. Dauphas & A. Pourmand 2011).

The formation pathway of Figure 4 implicitly assumes that primordial volatiles stored in the rocky interior of embryos are preserved during these two collisions. Consequently, the primordial ²²Ne concentration of the rocky interior of each embryo corresponds to that of the bulk mantle of the Earth, after correcting for mantle outgassing. A reasonable hypothesis would be that those impacts were capable of stripping the upper mantle of its primordial content, but spared the majority of the deep mantle reservoirs. This scenario would explain why primordial signatures of Ne are present in the deep mantle, while the Ne budget of the upper MORB mantle is consistent with a SWI origin, which could have been accreted after a giant impact (C. D. Williams & S. Mukhopadhyay 2019).

Even if either of the two impacts of Figure 4 lead to the loss of deep mantle volatiles, we argue that the gas would be recaptured by the merged body. We will assess this statement by first computing whether the ejected material would be able to complete a full orbit, forming a torus along the path of the merged body, before being blown away by the solar wind. We will also investigate whether this torus of ejected gas diffuses into the interplanetary medium before its accretion onto the newly formed protoplanet.

First, the dynamical pressure of the solar wind exerts an outward acceleration of

$$a_{\rm dyn} \sim \frac{2\pi a \delta l \rho_* v_*^2}{M_{\rm ejected}},$$
 (19)

where a is the orbital distance of 1 au, δl the width of the torus, ρ_* the volume mass density of solar wind, v_* its velocity, and $M_{\rm ejected}$ the total mass ejected by the impact. Here, the dynamical pressure of the solar wind $P_{\rm SW} \sim \rho_* v_*^2$ is estimated using average values at 1 au of $v_* \approx 376 {\rm km/s}$ and $\rho_* \approx 6~m_H {\rm cm}^{-3}$ (taken for the slow wind component in Table 4 of C. Larrodera & C. Cid 2020, neglecting alpha particles and heavier ions for simplicity). We set the width of the torus to $\delta l \sim v_{\rm esc}/\Omega$, where $v_{\rm esc} \equiv \sqrt{\frac{2GM_{\rm rock}}{R_{\rm rock}}} \sim 11.2 {\rm km/s} \left(\frac{M_{\rm rock}}{M_{\oplus}}\right)^{1/3}$ is the surface escape velocity of the embryo and Ω is the Keplerian frequency Ω at 1 au. Consequently, over a single orbit of the ejected material, its radial velocity would have grown relative to the Keplerian local orbital velocity $v_K \equiv a\Omega$ by

$$\frac{\Delta v}{v_K} \sim \frac{2\pi}{\Omega} \frac{a_{\rm dyn}}{v_K} \sim 1.3 \times 10^{-8} \left(\frac{M_{\rm rock}}{M_{\rm ejected}}\right) \left(\frac{M_{\oplus}}{M_{\rm rock}}\right)^{2/3}.$$
(20)

Second, the torus of ejected gas with width δl will diffuse on a timescale of

$$t_{\text{diff}} \gtrsim \frac{\delta l^2}{\nu},$$
 (21)

where ν is the kinematic viscosity of the gas. As the viscosity of nebular gas is uncertain (R. R. Rafikov 2017), we estimate with the molecular viscosity $\nu_{\rm mol} \sim v_{\rm th} \lambda/3$, where $v_{\rm th}$ and $\lambda \equiv 1/(\sqrt{2}n\sigma_{\rm mol})$ are the mean molecular speed and mean free path of the ejected medium, respectively, the latter set by the number density n of molecules in the torus and the molecular cross-section $\sigma_{\rm mol}$ (R. B. Bird et al. 2007). We express Equation (21) as a lower limit on t_{diff} because full diffusion would occur over the entire orbital distance a, so that t_{diff} can also be estimated as $\sim a^2/\nu$. We expect the random velocity of ejected particles to be comparable to the escape velocity of the merged embryos and therefore set $v_{\rm th} \sim v_{\rm esc}$. For simplicity, we further assume that n is constant in space, so that the ejected mass M_{ejected} of primordial gas with mean molecular weight $\mu_{\rm disk} \approx 2.37$ (ignoring compositional changes from disk values) is uniformly distributed over the volume of the torus $2\pi^2 a\delta l^2$. We adopt the cross section of H_2 , that is $\sigma_{\rm mol} \sim \sigma_{H_2} \approx 0.2 {\rm nm}^2$ (see reaction 46 of T. Tabata & T. Shirai 2000), representative of a H-dominated gas in a molecular regime. Under these assumptions, the timescale of diffusive loss is given by

$$t_{\rm diff} \gtrsim \frac{3}{\sqrt{2}\pi^2} \frac{\sigma_{\rm mol}}{av_{\rm esc}} \frac{M_{\rm ejected}}{\mu_{\rm disk} m_H},$$
 (22)

or

$$t_{\rm diff} \gtrsim 1.65 \times 10^9 {\rm yr} \Big(\frac{M_{\rm ejected}}{M_{\rm rock}}\Big) \Big(\frac{M_{\rm rock}}{M_{\oplus}}\Big)^{2/3}.$$
 (23)

For a proto-Earth doubling consisting of two $\sim 0.3 M_{\oplus}$ embryos merging into a $M_{\rm rock} \sim 0.6 - 0.7 M_{\oplus}$ proto-Earth, we can fix as a lower bound for M_{ejected} the envelope mass $M_{\rm env} \approx 2 \times 10^{-6} M_{\rm rock}$ (see Figure 3(c)) required to explain the deep mantle primordial Ne reservoir. Using $M_{\rm rock} = 0.65 M_{\oplus}$ for a representative case, Equations (20) and (23) give $\Delta v/v_K \sim 0.0089 \ll 1$ and $t_{\rm diff} \gtrsim 2500 {\rm yr}$. As such, primordial volatiles are unlikely to escape the orbit prior to their recapture by the formed protoplanet, instead being rapidly reaccreted and dissolved into its rocky interior, on timescales comparable to those shown in Figure 3. This calculation also shows that the concentration of nebular ²²Ne dissolved into embryos could not have initially exceeded our reference value of $c_{^{22}\text{Ne,p}} = (1.08 \pm 0.60) \times 10^{-13} \text{mol/g}$, reinforcing our tight upper constraint on the critical embryo mass of $\sim 0.3 M_{\oplus}$ found in Section 3.

4.3. Noble gas budget of the deep mantle

In this section, we discuss the current constraints on the origin of the deep-mantle budgets of He, Ne, Ar, Kr, and Xe, and whether our dissolution calculation aligns well with the broader understanding of these reservoirs. Along with the measurements of $c_{^{22}\mathrm{Ne,DM}}$ used as a reference in Section 3, B. Marty (2012) (see their Table 1) reported the concentrations of the non-radiogenic $^3\mathrm{He},^9$ $^{36}\mathrm{Ar},^{84}\mathrm{Kr},$ and $^{130}\mathrm{Xe}$ isotopes trapped in mineral lattice samples of the bulk (i.e. non-degassed) mantle, which we summarize in Table 1.

AX	$c_{ m A_{X,DM}} \; (m mol/g)$
³ He	$(5.7 \pm 3.6) \times 10^{-14}$
²² Ne	$(5.8 \pm 3.2) \times 10^{-15}$
$^{36}\mathrm{Ar}$	$(7.8 \pm 4.3) \times 10^{-14}$
⁸⁴ Kr	$(1.9 \pm 1.1) \times 10^{-15}$
¹³⁰ Xe	$(2.60 \pm 0.68) \times 10^{-17}$

Table 1. Noble gas concentrations $c_{A_{x,DM}}$ of non-radiogenic isotopes (^{A}X) of He, Ne, Ar, Kr and Xe reported by B. Marty (2012) for the Earth's bulk (i.e. non-degassed) mantle.

Although current plume samples (C. D. Williams & S. Mukhopadhyay 2019) strongly imply an inner mantle reservoir of Ne dominated by remnants of the solar nebula, the same cannot be assumed about the origin of the deep mantle reservoirs of the other noble gases. Nonetheless, the presence of nebular Ne dissolved in the mantle implies that other components of the protoatmosphere were similarly incorporated into the rocky interior during the chemical equilibration of the mantle-envelope boundary.

Given the concentration $c_{^{22}\mathrm{Ne,p}}$ of dissolved primordial $^{22}\mathrm{Ne}$ into the mantle at surface pressure P_0 , Henry's Law (Equation 12) can be used to compute the expected initial primordial concentration of an arbitrary species $^{\mathrm{A}}\mathrm{X}$:

$$c_{\rm AX,p} = \frac{k_{\rm Ne}}{k_{\rm X}} \frac{n_{\rm AX}}{n_{\rm ^{22}Ne}} c_{\rm ^{22}Ne,p}.$$
 (24)

Here, $k_{\rm X}$ and $n_{\rm AX}$ are the solubility constant and elemental abundance of species $^{\rm A}{\rm X}$, following the same format as for $^{22}{\rm Ne}$ in Equation (12). The relative concentrations of primordial volatiles $c_{\rm AX,p}$ dissolved in the

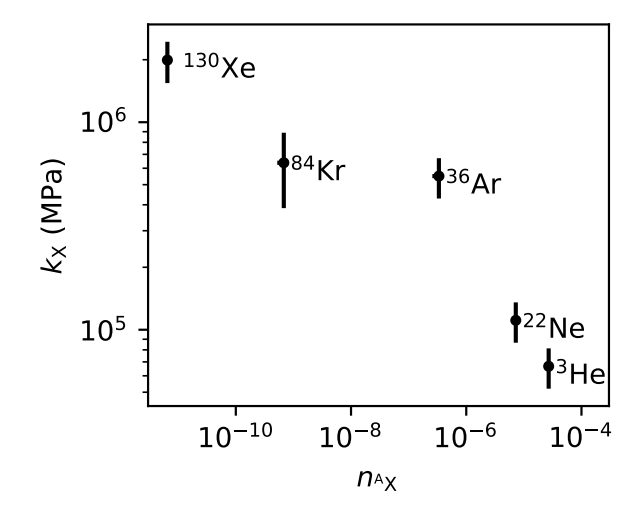


Figure 6. Dissolution parameters of 5 non-radiogenic isotopes ($^{\rm A}{\rm X}$) of nebular noble gases ($^{3}{\rm He}$, $^{22}{\rm Ne}$, $^{36}{\rm Ar}$, $^{84}{\rm Kr}$, and $^{130}{\rm Xe}$) into basaltic melt. The abundances of each isotopes $n_{\rm AX}$ are taken from the analysis of M. Asplund et al. (2021). We use the elemental values of Henry's constant $k_{\rm X}$ (See Equation 12) of G. Iacono-Marziano et al. (2010) for He, Ne and Ar and the ones of A. Jambon et al. (1986) for Kr and Xe, evaluated at the melting temperature of the melt $T_{\rm melt} \approx 1600{\rm K}$ (M. M. Hirschmann 2000; E. L. Tomlinson & T. J. B. Holland 2021).

mantle are therefore regulated by their primordial abundances in the solar nebula and their solubility in basaltic melts. As discussed in Section 2.2, the composition of the solar nebula has been constrained by spectroscopic analyses of the Sun's photosphere from M. Asplund et al. (2021), and the model of G. Iacono-Marziano et al. (2010) can once again be used, this time to compute the solubility constants of He and Ar. For Kr and Xe, we resort to the solubility constants measurements in basaltic melts of A. Jambon et al. (1986). In each case, we evaluate the constants at $T_{\rm melt} \approx 1600 {\rm K}$, typically associated with the final stage of the melt before solidification (M. M. Hirschmann 2000; E. L. Tomlinson & T. J. B. Holland 2021). The elemental abundances and solubility constants of ³He, ²²Ne, ³⁶Ar, ⁸⁴Kr and ¹³⁰Xe are presented in Figure 6, which shows that lighter noble gases are preferentially dissolved into basaltic melts.

The remainder of this section explores the implications of Figure 7, in which we compare the predictions of Equation (24) with the measured deep mantle concentrations of B. Marty (2012). In Section 4.3.1, we show that the solar-like He reservoir inferred from OIB samples is consistent with the dissolution of primordial nebular gas. Section 4.3.2 explains why similar conclusions cannot be drawn for Ar, Kr and Xe reservoirs, which appear to be mixtures of preserved early signa-

⁹ Although not directly reported by B. Marty (2012), the bulk mantle concentration of ³He can be recovered from their measurement of $c_{14}_{\rm N} = (9.0 \pm 4.6) \times 10^{-8} \, {\rm mol/g}, \, {\rm N/^{40}Ar} = 160 \pm 40,$ $^4{\rm He/^{40}Ar} = 1.9 \pm 0.5$ and the helium isotopic ratios of $^3{\rm He/^4He} \sim 5.18 \times 10^{-5}$ measured in Icelandic OIB samples (D. R. Hilton et al. 1999).

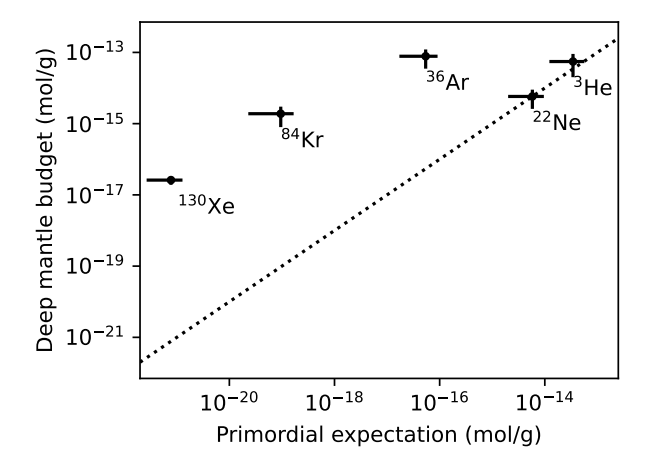


Figure 7. Comparison of the expected concentrations of primordial nebular gas dissolved in the mantle with the measured deep mantle concentrations measured by B. Marty (2012) in plume samples. A dotted one-to-one line centered on ²²Ne is shown to illustrate how the ³⁶Ar, ⁸⁴Kr and ¹³⁰Xe reservoirs cannot be purely explained by the capture of primordial volatiles as isotopic measurements argue is the case for Ne (C. D. Williams & S. Mukhopadhyay 2019) and most likely He (see Section 4.3.1).

tures of CI carbonaceous chondrites, contaminated by the subduction of gas from the Earth's secondary atmosphere. Finally, we summarize in Section 4.3.3 the current constraints on the noble gas content of the deep mantle, and present a simple calculation in which we explain the measurements of Table 1 with a mixture of nebular, chondritic, and subducted atmospheric gas.

4.3.1. Expected nebular deep mantle budget

In Figure 7, we report a $\approx 1\sigma$ agreement between the expected concentration of dissolved nebular ³He of $(3.4\pm2.2)\times10^{-14}{\rm g/mol}$ and its measured deep mantle budget of $(5.5\pm3.5)\times10^{-14}{\rm g/mol}$. This agreement is consistent with a nebular source for the deep mantle He, but a SWI origin cannot be excluded from analyses of ³He/⁴He ratios in OIB samples alone.

Indeed, He from the solar nebula and from SWI solids is characterized by ${}^{3}\text{He}/{}^{4}\text{He}$ values of $\approx 259R_{\rm A}$ and ${}^{3}\text{He}/{}^{4}\text{He} = (331.4 \pm 6.4)R_{\rm A}$, respectively (V. S. Heber et al. 2012), 10 with $R_{\rm A} = 1.4 \times 10^{-6}$ being the atmospheric ${}^{3}\text{He}/{}^{4}\text{He}$ value (Y. Sano et al. 1988). Determining which source is most consistent with the initial He isotopic composition of the deep mantle is challenging, mainly because the α -decay of heavy elements such as

U and Th produces additional ⁴He in the mantle, lowering the ³He/⁴He ratio of the primitive non-radiogenic source (J. M. D. Day et al. 2005; J. M. Day et al. 2015).

Mantle plumes found in Hawaii (P. J. Valbracht et al. 1997), Iceland (D. R. Hilton et al. 1999), the Galápagos Islands (M. D. Kurz et al. 2009) and Samoa (M. G. Jackson et al. 2009) do exhibit high ${}^{3}\text{He}/{}^{4}\text{He} \gtrsim 30R_{\text{A}}$ ratios (see J. M. Day et al. 2022, their Table 2) compared to the canonical MORB value of ${}^{3}\text{He}/{}^{4}\text{He} = 8 \pm 2R_{\text{A}}$ and the atmospheric value R_A , but relating these measurements to a precise source requires an understanding of how radiogenic He is produced in the Earth's silicate mantle (J. M. Day et al. 2022). As such, we limit ourselves to concluding from Figure 7 that our dissolution calculation of nebular Ne in the deep mantle as reported by C. D. Williams & S. Mukhopadhyay (2019) is consistent with the current knowledge of He from OIB samples.

4.3.2. Origins of heavy noble gases in the deep mantle

Figure 7 displays an excess of $^{36}\mathrm{Ar}$, $^{84}\mathrm{Kr}$ and $^{130}\mathrm{Xe}$ by factors of $\gtrsim 10^4$ compared to the nebular dissolution scenario. If nebular accretion cannot fully account for this excess in the deep mantle, what processes supply the heavy noble gas content?

First, CI carbonaceous chondrites are the most volatile-rich primitive meteorites known in the solar system (G. W. Kallemeyn & J. T. Wasson 1981), and were incorporated into the Earth during its assembly (R. O. Pepin 1991; B. Marty 2012; A. N. Halliday 2013). They carry most of their noble gases in a carrier phase called the "Q-component" (originally named for "quintessence" by R. S. Lewis et al. 1975) with chemical and isotopic compositions distinct from solar values, enriched in heavy noble gases (U. Ott 2002). The preferential capture of heavy species in CI chondrites is due to the carbonaceous material of the Q-phase efficiently trapping heavy volatiles (e.g. Ar, Kr, Xe, H₂O, C, N) over their formation in the volatile-rich conditions of the early solar system (R. Wieler et al. 1991, 1992; H. Busemann et al. 2000).

Second, the recycling of atmospheric volatiles via dissolution in the oceanic lithosphere and subsequent subduction in the Earth's interior is an efficient carrier of heavy noble gases (C. J. Ballentine & D. N. Barfod 2000; G. Holland & C. J. Ballentine 2006; M. A. Kendrick et al. 2011; S. Mukhopadhyay & R. Parai 2019). Although this contamination from the Earth's secondary atmosphere is not a viable source of light noble gases (He, Ne) due to their poor solubility in seawater (M. A. Kendrick et al. 2018), recent isotopic analysis of Galápagos and Iceland OIB samples along with realistic recycling calculations by S. Peron & S.

¹⁰ These associated values from V. S. Heber et al. (2012) assume that isotopic compositions of the primordial nebula is consistent with the Sun's photosphere and the SWI solids with bulk solar wind measurements.

Mukhopadhyay (2022) argued that significant fractions of Kr and Xe found in the deep mantle (in the concentrations shown in Table 1) are of atmospheric provenance.

For Kr, approximately half of the deep mantle reservoir is isotopically consistent with air (S. Péron et al. 2021). Disentangling primitive Kr signatures from atmospheric contamination requires high-precision isotopic measurements (e.g., see Figure 2 of A. N. Halliday 2013). As illustrated in Figure 7, the non-atmospheric half of the Kr budget is unlikely to originate from the solar nebula, and A. N. Halliday (2013) concluded from their analysis of ⁸⁴Kr/³⁶Ar in the deep Earth that it can be explained by the incorporation of CI carbonaceous chondrites during the Earth's, or its parent bodies', assembly. The relative ratio of $^{84}\mathrm{Kr}/^{22}\mathrm{Ne} = 2.7 \pm 3$ (see Tables 2, 3, and 4 of U. Ott 2002) in the Qcomponent of CI chondrites is much greater than the value of $^{84}\mathrm{Kr}/^{22}\mathrm{Ne} = (1.6 \pm 0.9) \times 10^{-5}$ expected by the nebular dissolution scenario (see Figure 7). Consequently, an initial Kr reservoir provided by CI chondrites would account for the large excess of ⁸⁴Kr in the deep mantle while contributing negligibly to its Ne budget.

Several studies of chondritic signatures in the atmosphere and upper mantle (e.g., see R. J. Walker 2009, for a review) have linked the acquisition of chondrites to a late veneer (J. W. Morgan et al. 2001; G. Holland et al. 2009). On the contrary, the same cannot be assumed for Kr signatures in the deep mantle (B. Marty 2012), which is largely isolated from late veneer contributions (see Figure 4 of C. L. Harper & S. B. Jacobsen 1996, for a schematic illustration of the evolution of the Earth's accretion of chondrites/planetary in its global core-mantle-atmosphere system). From their measurements of Kr isotopes in Galapagos and Iceland plumes, S. Péron et al. (2021) concluded that Kr from CI chondrites must have been delivered in the early accretion phases of the Earth, before the lower mantle differentiated itself from the upper layers and preserved its initial signatures. In fact, the coexistence of nebular Ne and chondritic Kr in the deep mantle implies that CI chondrites were absorbed by the Earth in its earliest stages of accretion, in the presence of the solar nebula (M. W. Broadley et al. 2020).

This conclusion can easily be reconciled with our favored formation scenario (Figure 4), simply by assuming that CI chondrites were primarily incorporated into $\sim 0.3 M_{\oplus}$ Earth embryos as they formed their rocky interior, prior or simultaneously to their accretion of a primordial envelope and the dispersal of the disk gas. An apparent objection to this idea is that solid chondrites likely formed in the colder, outer regions of the solar system (E. Anders & N. Grevesse 1989; G. W. Kalle-

meyn et al. 1994; K. Lodders 2003) and would have had to migrate to ~ 1 au within the lifetime of the disk to be integrated in the rocky interior of Earth embryos. However, S. N. Raymond & A. Izidoro (2017) argued from their dynamical simulations of the early solar system that the implantation of outer planetesimals, rich in carbonaceous chondrites, is a direct consequence of the formation and migration of the giant planets, as dictated by the Grand Tack model (B. M. S. Hansen 2009) during Jupiter's rapid gas accretion phase, therefore in the presence of the gas disk (see also D. P. O'Brien et al. 2014). The inclusion of such chondrite-rich planetesimals in Earth embryos would explain the primitive Kr reservoir of the deep mantle, under the planetesimal accretion scenario. Furthermore, the chondrules themselves are small 0.01-10mm (E. Scott & A. Krot 2007) enough to be efficiently transported to the inner solar system via aerodynamic radial drift (S. J. Weidenschilling 1977; Y. Nakagawa et al. 1986), which supports their early incorporation into solid grains under the pebble accretion framework.

For Xe, the deep mantle reservoirs are even more affected by atmospheric contamination, accounting for more than 90% of the Xe total concentration (S. Peron & S. Mukhopadhyay 2022) and almost entirely overprinting any primordial Xe signature. It is still generally understood that the Xe content found in the mantle also constitute a mixture of subducted atmospheric gas (G. Holland & C. J. Ballentine 2006) and a minor ($\leq 10\%$ according to S. Peron & S. Mukhopadhyay 2022) primitive chondritic component (M. Pujol et al. 2011). This is quite unexpected, as the atmospheric ¹³⁰Xe/⁸⁴Kr ratio is about one order of magnitude lower than that of CI chondrites (R. O. Pepin 1991; R. O. Pepin & D. Porcelli 2002; N. Dauphas 2003; D. V. Bekaert et al. 2020), implying that a significant fraction of the expected chondritic Xe is "missing" (see Figure 7 of B. Marty 2012).

Many mechanisms have been invoked to explain this apparent Xe deficit, including the sequestration of Xe in minerals at high pressure (C. Sanloup et al. 2005), preferential fractionation of Xe isotopes due to its low ionization potential (T. J. Bernatowicz & A. J. Fahey 1986; K. V. Ponganis et al. 1997; C. M. Hohenberg et al. 2002; Y. Marrocchi et al. 2011), hydrodynamic escape early in the Earth's history (R. O. Pepin 1991; R. O. Pepin & D. Porcelli 2002), and significant Xe-loss from giant impacts (G. W. Wetherill 1975; R. O. Pepin 1997; D. Porcelli et al. 2001). The latter two scenarios, however, appear unlikely since the release of Xe would have been accompanied by similar losses of the lighter noble gases, which is not reported in OIB samples (B. Marty 2020).

Together with the sequestration of Xe and its low ionization potential, another viable rational is the preferential partitioning of Xe in the iron core of the Earth. As investigated by K. Wang et al. (2022), the early formation of the outer core via the segregation of liquid iron from magma oceans is expected to have entrained volatiles in the iron core. The relative concentration of each noble gases expected in primordial reservoirs within the liquid core would be set by their metal/silicate partition coefficients D. Xe is expected to be more siderophile than Kr in rocky interiors, with a preferential partitioning ratio of $D_{\mathrm{Xe}}/D_{\mathrm{Kr}} \approx 17.5$ (See Figure 2 of K. Wang et al. 2022). 11 The Xe "paradox" in the deep mantle could therefore be solved simply by most of the missing primitive Xe reservoir being incorporated in the iron core during early formation, as we argue in Section 4.3.3.

Finally, the origins of Ar in the deep mantle are more uncertain, with mantle reservoirs heavily dominated by the radiogenic ⁴⁰Ar isotope, produced by the decay of ⁴⁰K in the rocky interior and then outgassed in the atmosphere (M. L. Bender et al. 2008). Argon is by far the most prominent noble gas in the atmosphere, accounting for 0.934mol% of the atmospheric composition, making it more likely to dissolve into seawater and subduct in the Earth's interior.

Recovering an initial component using the relative abundances of the non-radiogenic 36 Ar and 38 Ar within the resulting 40 Ar dominated mixture remains a challenge, and will likely require further samples and high-precision isotopic analyses (J. M. Day et al. 2022). In fact, the measured 38 Ar/ 36 Ar ratios of MORB and OIB samples are consistent with both atmospheric and chondritic values (A. Raquin & M. Moreira 2009; S. Peron et al. 2017). Hence, any solar-like primordial signatures of Ar must have been obscured by the incorporation of chondrites and/or subducted atmospheric gas.

In their discussion of subducted recycled noble gases, S. Peron & S. Mukhopadhyay (2022) hypothesized fractions of recycled non-radiogenic Ar ranging from 14% to 50%. They proposed these values to reflect a continuous range between the primitive Ne reservoir which shows no evidence of significant atmospheric contamination (C. D. Williams & S. Mukhopadhyay 2019) and the

approximate half of the Kr budget which is not sourced by CI carbonaceous chondrites but by subduction of air, as inferred from Kr isotopic measurements (A. N. Halliday 2013; S. Péron et al. 2021). Other studies argue that the fraction of subducted atmospheric Ar should be similar to that of Xe, with estimated values of $\sim 93\%$ and even 100% estimated by G. Holland & C. J. Ballentine (2006) and C. D. Williams & S. Mukhopadhyay (2019), respectively. The current lack of constraints on non-radiogenic Ar makes it a particularly poor tracer of the initial inventory of the deep mantle.

4.3.3. A self-consistent deep mantle noble gas budget?

In Figure 8, we summarize our discussion of noble gases in the deep mantle by presenting a simple estimation of the contributions of each source of the non-radiogenic 3 He, 22 Ne, 36 Ar, 84 Kr, and 130 Xe. For comparison purposes, the contributions are normalized to the measured concentrations $c_{\rm AX,DM}$ of B. Marty (2012) presented in Table 1 and can therefore be expressed as relative fractions (e.g., $f_{\rm ^{84}Kr,CI} \equiv \frac{c_{\rm 8^4Kr,CI}}{c_{\rm 8^4Kr,DM}}$ for the fraction of the deep mantle 84 Kr coming from CI chondrites). The figure is created as follows:

1. We first fix the fractions $f_{AX,atm}$ of each species ^AX accounted for by the subduction of atmospheric gas to the deep mantle. For Kr and Xe, we adopt the values reported by S. Peron & S. Mukhopadhyay (2022) in Icelandic plume sources of $f_{^{84}\text{Kr,atm}} = 64 \pm 8\%$ and $f_{^{132}\text{Xe,atm}} = 95.4_{-5.5}^{+4.6}\%$, respectively. 12 As mentioned in Section 4.3.1, ³He and ²²Ne in the deep mantle are expected to be primordial with little to no contamination from the Earth's secondary atmosphere, and we consequently assume for simplicity that these reservoirs are purely primitive (i.e. $f_{^3\mathrm{He,atm}} \approx f_{^{22}\mathrm{Ne,atm}} \approx$ 0). Because the exact balance of the ³⁶Ar budget between CI chondrites and subducted atmospheric gas remains uncertain, we fix a value of $f_{^{36}\mathrm{Ar,atm}} \approx 18\%$ to directly match the reported concentration of ³⁶Ar by B. Marty (2012), which is chosen after constraining the contribution from CI chondrites in the next step. This choice is quite arbitrary as the large uncertainty in the ³⁶Ar measurement of B. Marty (2012) allows fractions ranging from 0% to 73%.

¹¹ K. Wang et al. (2022) report partition coefficients as functions of temperature, which for our study would have to be set to the core-mantle boundary temperature of early $\sim 0.3 M_{\oplus}$ Earth embryos, the calculation of which is beyond the scope of this work. For simplicity, we evaluate $D_{\rm Xe}/D_{\rm Kr}$ at 2500K and note that variations in its value are small ($\lesssim 50\%$) over the temperature regime (2300K ≤ $T \le 5000$ K) studied by K. Wang et al. (2022).

 $^{^{12}}$ Those measurements should be treated as upper bounds, as the analogous Galápagos OIB samples exhibit lower fractions of subducted atmospheric material of $f_{\rm ^{84}Kr,atm}=48\pm8\%$ and $f_{\rm ^{132}Xe,atm}=93.4\pm4.6\%.$

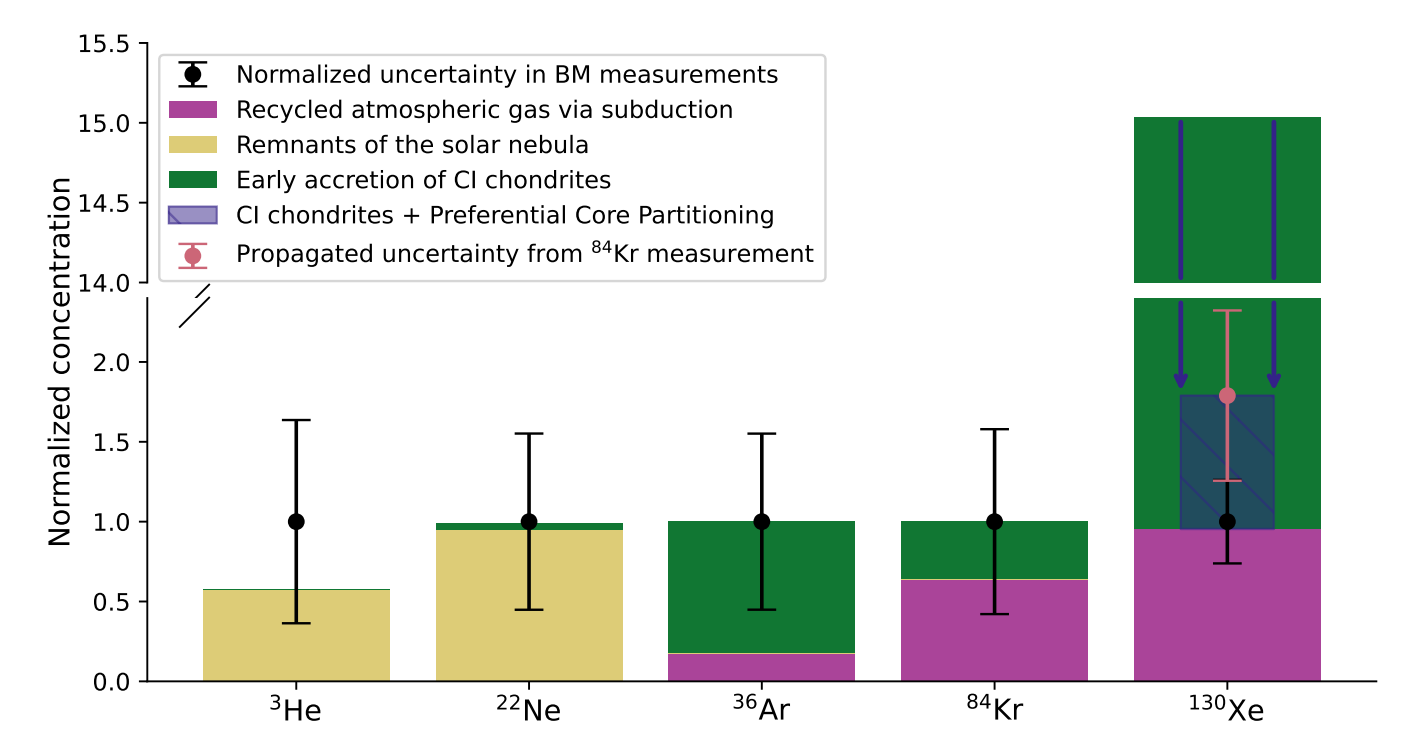


Figure 8. Estimates of the noble gas sourcing in the deep mantle reservoirs of ³He, ²²Ne, ³⁶Ar, ⁸⁴Kr, and ¹³⁰Xe. Contributions from dissolved primordial gas from the solar nebula, CI carbonaceous chondrites incorporated during early formation of rocky interiors and recycled gas subducted from the Earth's secondary atmosphere are represented in yellow, green and magenta, respectively. Concentrations are normalized to the measurements of noble gas concentrations in the bulk mantle (BM) of the Earth reported by B. Marty (2012), with the uncertainty on those measurements shown in black. Due to the preferential partitioning of Xe into the core with respect to Kr (K. Wang et al. 2022), the expected fraction of the initial ¹³⁰Xe chondrite contribution is reduced and shown with a small inset blue bar, with the propagated uncertainty from the ⁸⁴Kr measurement shown in pink.

2. Next, we anchor $f_{^{84}\mathrm{Kr,CI}}$ to $100\% - f_{^{84}\mathrm{Kr,atm}} \approx 36\%$, attributing the remaining reservoir of $^{84}\mathrm{Kr}$ to CI chondrites as argued in Section 4.3.2. Based on the relative abundances $\binom{^{A}\mathrm{X}}{^{84}\mathrm{Kr}}\binom{^{}}{^{}}$ of each noble gas $^{A}\mathrm{X}$ with respect to $^{84}\mathrm{Kr}$ in the primary Q component of CI chondrites (computed from Tables 2, 3, and 5 of U. Ott 2002), we calculate the expected fraction of the other noble gas reservoirs that would consequently originate from chondrites, as given by

$$f_{\rm ^{A}X,CI} \approx f_{\rm ^{84}Kr,CI} \frac{c_{\rm ^{84}Kr,DM}}{c_{\rm ^{A}X,DM}} \left(\frac{\rm ^{A}X}{\rm ^{84}Kr}\right)_{\rm CI}.$$
 (25)

Equation (25) gives fractions of $f_{^{3}\mathrm{He,CI}} = 0.080 \pm 0.055\%$, $f_{^{22}\mathrm{Ne,CI}} = 4.4 \pm 2.9\%$, $f_{^{36}\mathrm{Ar,CI}} = 82 \pm 51\%$ and $f_{^{130}\mathrm{Xe,CI}} = 1410 \pm 830\%$. The remarkably high value of $f_{^{130}\mathrm{Xe,CI}}$ expected from Equation (25) emphasizes the "paradoxal" Xe deficit in the deep mantle. We reconcile this disagreement by correcting to $f_{^{130}\mathrm{Xe,CI}} \approx 81 \pm 48\%$ for the preferential partitioning of Xe in the iron core compared to Kr, given by $D_{\mathrm{Xe}}/D_{\mathrm{Kr}} \approx 17.5$ (K. Wang et al. 2022).

3. Finally, we assume a 22 Ne budget primarily dominated by remnants of the primordial solar nebula with $f_{^{84}\text{Ne,p}} = 95.6\%$, taking into account the small $\sim 4.4\%$ chondritic 22 Ne contribution retrieved in the previous step. Using Equation (24) for normalized contributions then gives $f_{^{3}\text{He,p}} = 58 \pm 37\%$, $f_{^{22}\text{Ar,p}} = 0.066 \pm 0.045\%$, $f_{^{36}\text{Kr,p}} = 0.0048 \pm 0.0036\%$ and $f_{^{130}\text{Xe,p}} = 0.0028 \pm 0.0019\%$.

On the whole, Figure 8 shows that the noble gas budgets of the deep mantle can be reconciled by a combination of dissolved nebular gas, incorporation of CI carbonaceous chondrites, and subducted atmospheric material, without invoking the inclusion of SWI material. We conclude that light noble gases in the deep mantle reflect the gas dissolution of early Earth embryos while heavy noble gases complementarily probe the Earth's solid accretion history.

Assuming CI carbonaceous chondrites supplied the primitive Ar, Kr and Xe reservoirs, a small ($\sim 5\%$) imprint of CI chondrites may be present within the otherwise nebular Ne content. Such a contribution would not significantly affect the measurements of C. D. Williams

& S. Mukhopadhyay (2019), which allow a maximum of 10-15% of the Ne reservoir to be of either atmospheric or chondritic origin (S. Peron & S. Mukhopadhyay 2022).

Lastly, Figure 8 also demonstrates that the preferential partitioning of Xe in the Earth's iron core is a viable solution to the missing Xe problem in the deep mantle, reconciling to $\approx 1\sigma$ the measured concentration of Kr and Xe of B. Marty (2012). A caveat to this last conclusion is that we have ignored the similar preferential partitioning of He, Ne and Ar. Their incorporation rate varies much more with temperature (see Figure 2b of K. Wang et al. 2022) and is harder to approximate without a complete model of the interior structure of planetary embryos.

We caution against drawing firm conclusions from this simple attempt at reconciling the measurements of He, Ne, Ar, Kr, and Xe in OIB samples, especially in light of the large uncertainties on deep mantle volatile measurements (B. Marty 2012; A. N. Halliday 2013). More precise measurements and detailed models of planetary interior dynamics beyond the scope of this work are needed to further constrain a self-consistent narrative for the origins of all five noble gas reservoirs (He, Ne, Ar, Kr, and Xe).

4.4. Primordial dissolution of hydrogen

The capture of primordial atmospheres atop the molten surface of Earth embryos delivers H₂ to their interior, consistent with the dissolution of noble gases. The chemical interactions of nebular H₂ with silicate species such as MgO, SiO₂, MgSiO₃, FeO, MgSiO₃ prevents us from using H as a probe of early accretion processes, but its delivery to the rocky interior of Earth embryos may explain several of the Earth's key features (E. D. Young et al. 2023).

First, once incorporated into the mantle, hydrogen can be converted to water through its interactions with silicates. As such, a nebular origin is a plausible explanation of the Earth's water content (H. Genda & M. Ikoma 2008). Second, the Earth's outer (F. Birch 1964) and inner (A. Jephcoat & P. Olson 1987; L. Stixrude et al. 1997) cores are significantly less dense than pure Fe, by $\approx 10\%$ (R. Jeanloz 1979) and $\sim 3 - 6\%$ (W. W. Anderson & T. J. Ahrens 1994), respectively. This core density deficit implies the presence of light volatiles in the metal core, with C, H, O, S and Si as the most likely candidates (see J.-P. Poirier 1994, for a review). Once H₂ is dissolved into the mantle, T. Okuchi (1997) argued that $\gtrsim 95\%$ of the freshly formed water should have reacted with iron, partitioning H to the metal core and possibly accounting for up to 60% of the core density

deficit. Lastly, following nebular dispersal, H_2 degasses from the mantle and is subsequently lost by hydrodynamic escape. Because H_2 acts as a reducing agent, Z. D. Sharp (2017) inferred that its removal increases the Earth's bulk oxidation state, consistent with the mantle being highly oxidized.

Using a thermodynamical model of the chemical interactions of primordial atmospheres and magma oceans, E. D. Young et al. (2023) showed that these three geochemical constraints can consistently be explained by the chemical equilibrium of volatiles (O, H, C) at the interface of the atmosphere and the magma. Starting with $0.2-0.5M_{\oplus}$ Earth embryos of similar structure (see their Figure 3) to that of Figure 1, they found that initial H₂ primordial envelopes making up 0.2\% of the total embryo mass would approximately produce one terrestrial ocean and a metal density deficit of 8%, with final oxidation states consistent with the bulk silicate Earth. In light of the results presented in Section 3, a natural question to ask is whether the favored setting of E. D. Young et al. (2023) also reproduces the abundance of nebular ²²Ne reported by C. D. Williams & S. Mukhopadhyay (2019) in the deep mantle.

In Figure 9, we compare the initial conditions (prior to the exchange of H with the mantle) of the atmosphere used by E. D. Young et al. (2023) to obtain their solution with our gas accretion calculation. We only present our results for $f_{\rm dep}=10^{-3}$ since they are in agreement with the input parameters of $M_{\rm env}/M_{\rm core}\approx M_{\rm env}/M_{\rm p}=0.2\%,\, T_0=2350{\rm K},\, {\rm and}$

$$\left(\frac{P_0}{1 \text{ MPa}}\right) = 1.2 \times 10^5 \frac{M_{\text{env}}}{M_p} \left(\frac{M_p}{M_{\oplus}}\right)^{2/3},$$
 (26)

used by E. D. Young et al. (2023) for their $0.5M_{\oplus}$ solution.¹³ Even though they only present their results for $0.5M_{\oplus}$ embryos, they state that their conclusions are not critically dependent on embryo mass, as long as it exceeds $0.2M_{\oplus}$ allowing the presence of magma oceans (as we consistently observe in Figure 3(b)). By contrast, with the realistic treatment of the cooling of primordial envelopes developed in Section 2.1, we find that primordial envelopes atop $M_{\rm rock} \lesssim 0.4M_{\oplus}$ embryos would accrete and cool too efficiently to maintain magma oceans at their surface before they reach $M_{\rm env}/M_{\rm rock} \sim 0.2\%$. Consequently, the results of E. D. Young et al. (2023)

 $^{^{13}}$ We note that the values of P_0 obtained from our accretion model are smaller (by $\lesssim 10\%$) than the approximate scaling of Equation (26), which results in a negligible offset in the dissolved concentrations reported in the lower panel of Figure 9. We also note that solar-metallicity gas with $\mu_{\rm disk}\approx 2.37$ is considered in this work while E. D. Young et al. (2023) initialized their model with a 99.9mol% H envelope of $\mu=2.04$.

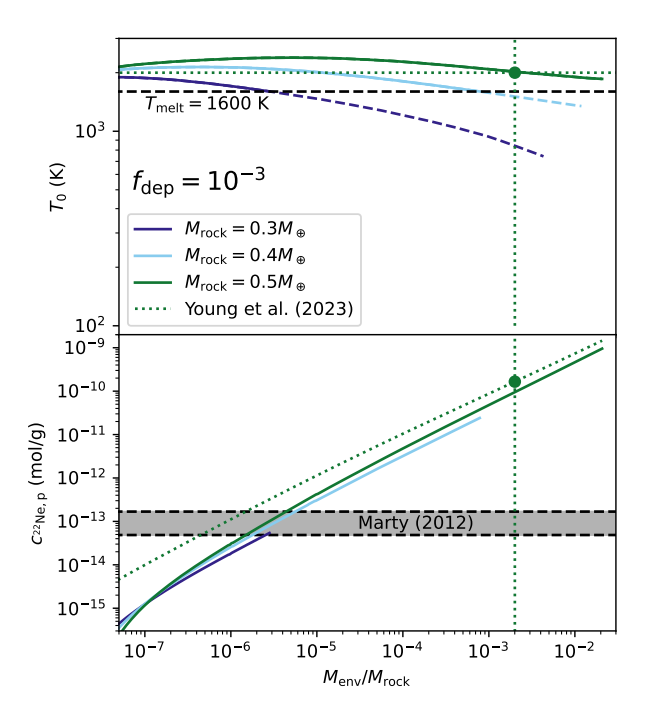


Figure 9. Surface temperature T_0 (upper panel) between the basaltic mantle of Earth embryos and primordial gas envelopes, along with the resulting concentration of primordial neon $c_{^{22}\mathrm{Ne,p}}$ dissolved in the mantle (lower panel), both as functions of $M_{\rm env}/M_{\rm rock}$. We compare the input atmospheric parameters and the resulting dissolved neon content (given by Equation 12) of the solution reported by the thermodynamic model of E. D. Young et al. (2023) (dots and dotted curves) with our results for rocky interior of masses $M_{\text{rock}} = [0.3, 0.4, 0.5] M_{\oplus}$ in blue, cyan and green, respectively. The embryos are embedded in a minimum-mass solar nebula of gas density depleted by a factor $f_{\rm dep} = 10^{-3}$ (see Equation 8). Volatiles are only dissolved in the presence of surface magma oceans (solid curves), that is when T_0 is greater than the melting temperature of basalt $T_{\rm melt} \approx 1600 {\rm K}$ (V. S. Solomatov & L. N. Moresi 2000), displayed with a black dashed curve. Once the surface of the mantle solidifies (colored dashed curves), atmospheric volatiles no longer dissolve in the solid surface of the rocky interior. We only show envelope masses corresponding to $t \lesssim 10 \text{ Myr}$, before envelope growth is cut short by the dispersal of the disk. The target concentration of primordial neon required to explain the measurements of B. Marty (2012) is shown with a gray shaded band.

can only be reconciled with the thermal evolution of primordial envelopes of $\sim 0.5 M_{\oplus}$ embryos and cannot be consistently translated to lower embryo masses.

This last conclusion further complicates the overall picture of the formation of the Earth. As shown in Figure 9, the existence of $\sim 0.5 M_{\oplus}$ embryos accreting and dissolving primordial gas from the solar nebula would drastically overpredict the target concentration expected from the bulk mantle measurements of

B. Marty (2012). Thus, one clear implication emerges: if the Earth's water and density deficit were primarily sourced by the dissolution of primordial H, the deep mantle should contain about ~ 1000 times more primordial Ne than observed. Conversely, a level of hydrogen dissolution consistent with the neon constraints of C. D. Williams & S. Mukhopadhyay (2019) would be insufficient to account for Earth's water content and a large fraction of the core density deficit, requiring complementary sources of water.

This tension could be resolved by departing from primordial H dissolution as the source of the bulk of the Earth's water, with the early accretion of water-rich solids and a late delivery via ice-rich comets as viable alternatives (H. Genda 2016). It may also be that there is a significant local deviation in disk composition from solar values.

4.5. Cooling and mixing of the mantle

In building the gas accretion models presented in Section 2, we assumed that volatiles dissolved at the surface of magma oceans are instantly delivered to the deep mantle. This choice can reasonably be justified if the radial mixing of the molten mantle is faster than the rate at which volatiles are delivered to the interior. To assess the validity of this assumption, we consider the mantle convective velocity $v_{\rm con}$, as given by (C. H. B. Priestley 1957, 1959; V. S. Solomatov 2000):

$$v_{\rm con} = 0.6 \left(\frac{\alpha g F_0 \Delta R}{\bar{\rho} c_P}\right)^{1/3}.$$
 (27)

Here, $\alpha=3\times 10^{-5}~{\rm K}^{-1}$ is the thermal expansivity (L. Elkins-Tanton 2008), $g=982{\rm cm/s^2}\left(\frac{M}{M_{\oplus}}\right)^{1/3}$ is the standard surface acceleration of embryos of constant bulk density $\bar{\rho}\equiv\frac{3M_{\oplus}}{4\pi R_{\oplus}^3}\approx 5.5{\rm g/cm^3},~F_0\equiv\frac{L}{4\pi R_{\rm rock}^2}$ is the flux from the atmosphere driving mantle convective flows, with the mantle convective luminosity set to that of the atmosphere L, and $\Delta R\equiv R_{\rm rock}-R_{\rm core}$ is the radial extent of the mantle, which is the relevant convective length scale, and $c_P=1.2561\times 10^7{\rm erg/g/K}$ is heat capacity of the mantle (L. Elkins-Tanton 2008). The coremantle structure of Earth embryos is hardly constrained, and we thus simply estimate ΔR by scaling down the radial extent of the Earth reported by C. J. Young & T. Lay (1987), assuming a constant bulk density $\bar{\rho}$, similar relative metal-silicate compositions and a complete differentiation of Fe to form an iron core:

$$\Delta R \sim 0.45 R_{\oplus} \left(\frac{M_{\text{rock}}}{M_{\oplus}}\right)^{1/3} = 0.45 R_{\text{rock}}.$$
 (28)

For the embryos considered in this work, we find that convective velocities as given by Equation (27) are expected to be on the order of

$$v_{\rm con} \sim 3400 \text{ cm/s} \left(\frac{L}{10^{30} \text{erg/s}}\right)^{1/3}.$$
 (29)

which corresponds to a mixing timescale $\tau_{\rm mix} \equiv \Delta R/v_{\rm conv}$ of

$$\tau_{\rm mix} \sim 0.0027 \text{ yr} \left(\frac{10^{30} \text{erg/s}}{L}\right)^{1/3} \left(\frac{M_{\rm rock}}{M_{\odot}}\right)^{1/3}, \quad (30)$$

or $\sim 0.0018 \rm yr$ for the favored $\sim 0.3 M_{\oplus}$ solution with spatially constant luminosity of $L \sim 10^{30} \rm erg/s$ found in our calculations.

In light of this estimate, the short accretion timescale of $10^{-5} {\rm yr} \lesssim t_{\rm acc} \lesssim 10^{-2} {\rm yr}$ over which the required $^{22} {\rm Ne}$ concentration is accreted (see Figure 3(c)) may warrant additional investigation. Since we find that gas accretion and mantle mixing operate on comparable timescales, a more detailed geodynamical approach to the convective motion of the mantles of Earth embryos may be required when modeling their interactions with primordial atmospheres. However, as discussed in Section 4.1.2, the primordial gas accretion depicted in Figure 3 for dust-free envelopes may be slowed by factors of up to ~ 1000 in the presence of dust grains, which may not have been completely cleared when the disk density reaches $f_{\rm dep} \sim 10^{-4} - 10^{-2}$.

The dissolution model presented in this work also assumes that the molten mantle surface remains in permanent thermal equilibrium with the base of accreted primordial envelopes. This choice simplifies the calculation by allowing the mantle surface temperature T_0 used for the dissolution calculation of Section 2.2 to be directly set to the value $T(R_{\rm rock})$ recovered from the accretion calculation (see Figure 2). This assumption implicitly relies on two conditions.

First, the mantle of the favored $\sim 0.3 M_{\oplus}$ Earth embryos must begin in a molten state with values of T_0 comparable to the initial temperature $T(R_{\rm rock}) \sim 2000 {\rm K}$ found at the bottom of the primordial envelopes of Figure 3(c). While quantitatively estimating T_0 for rocky interiors emerging from the nebula (i.e. for the first stage of Figure 4) is challenging, it is reasonable to assume that they could have emerged with $T_0 \gtrsim 2000 {\rm K}$, considering the $\gtrsim 1600 {\rm K}$ temperatures at which smaller $\sim 100-500$ km planetesimals are expected to reach over their early accretion (Y. Ricard et al. 2017; E. Kaminski et al. 2020; K. H. Dodds et al. 2021).

Second, as the atmosphere accretes and cools, the mantle must be able to rapidly shed its thermal energy to maintain the $T_0 = T(R_{\rm rock})$ equilibrium. The mantleenvelope surface adjusts itself to thermal changes ΔT at the base of the atmosphere on timescales

$$\tau_{\rm th} \sim \frac{M_{\rm mantle} c_p \Delta T}{L},$$
(31)

where $M_{\rm mantle}$ is the total mass of the silicate mantle. We expect the interior of primordial embryos to follow the structure of Figure 1, but the exact fraction of their mantle with respect to the total mass of $\sim 0.3 M_{\oplus}$ is uncertain. We can assume for simplicity that the interior of embryos follows an Earth-like structure with $M_{\rm mantle} \approx 67.5\% M_{\rm rock}$ (O. Sorokhtin et al. 2011). Therefore, for $\sim 0.3 M_{\oplus}$ embryos with retrieved luminosity values of $L \sim 10^{30}~{\rm erg/s}$, thermal balance is achieved within

$$\tau_{\rm th} \sim 0.46 \text{ yr} \frac{\Delta T}{1000 \text{K}}.$$
 (32)

Beginning from the initial thermal state $(T_0 \sim 2000 \text{K})$ of primordial envelopes atop $\sim 0.3 M_{\oplus}$ rocky interiors in Figure 3(c), the base of the envelope cools by $\Delta T \sim 400 \text{K}$ before reaching the solidification temperature of basalt $T_{\text{melt}} \approx 1600 \text{K}$. As such, the corresponding estimate of $\tau_{\text{th}} \sim 0.18 \text{yr}$ given by Equation (32) suggests a slow thermal response from the mantle compared to t_{acc} . Magma oceans may persist longer than what we expect from Figure 3, though this extension has little impact on the $0.3 M_{\oplus}$ solution, with increases to the dissolved neon concentration $c_{^{22}\text{Ne,p}}$ of $\lesssim 2$. Longer-lived magma oceans may increase $c_{^{22}\text{Ne,p}}$ enough to improve the marginal $0.2 M_{\oplus}$ solution reported in Figure 3(b) and strengthen the case against massive $\gtrsim 0.4 M_{\oplus}$ Earth embryos in the gas disk.

Overall, future studies of mantle-envelope exchanges of primordial volatiles in early Earth embryos would benefit from more detailed considerations of mantle thermodynamics to provide a more robust complete argument, but such considerations lie beyond the scope of this work.

5. CONCLUSION

Based on the discovery of primordial remnants of the solar nebula preserved in the Earth's deep mantle, we have presented a gas accretion and dissolution calculation which models the thermal evolution of the primordial gas envelopes of early Earth embryos, linking their formation environment to the planet's deep mantle ²²Ne reservoir. Based on our results, the most consistent formation scenario of the Earth proceeds as follows:

1. Earth embryos of mass $\sim 0.3 M_{\oplus}$ emerge as the primordial solar nebula is dispersing, at a time when

its gas density is depleted from MMSN values by a factor of 0.01% to 1%. Each of these embryos accretes a thin primordial gas envelope from the gas disk.

- 2. The existence of molten magma allows the delivery of primordial volatiles to the rocky interior of embryos. The dissolution of primordial gas is stopped by the rapid solidification of the atmosphere-mantle surface, after $10^{-5} \text{yr} \lesssim t_{\text{acc}} \lesssim$ 10^{-2} yr if gas accretion occurs in a dust-free regime or after $10^{-2} {\rm yr} \lesssim t_{\rm acc} \lesssim 10 {\rm yr}$ in the presence of dust grains. Remnants of this primordial volatile reservoir explains the nebular Ne signature measured in the deep mantle.
- 3. Starting from a set of three $\sim 0.3 M_{\oplus}$ embryos, the final assembly of the Earth post-disk dispersal occurs in a series of two mergers, consistent with current models of the Earth's growth through giant impacts.
- 4. The deep mantle reservoirs of He and Ne can be attributed to the dissolution of nebular gas in the rocky interiors of embryos, but the non-radiogenic components of Ar, Kr and Xe require an additional source, most likely the inclusion of CI carbonaceous chondrites early in the solid assembly of the embryos.
- 5. The ingassing of a nebular atmosphere would deliver H to the interior of embryos and produce water through its interaction with mantle silicates. However, the primordial atmospheres required to explain the deep mantle primordial reservoir of Ne are ~ 1000 times less massive than those invoked by modern geochemistry models to explain the Earth's water and core density deficit.

Our conclusions reflect the best constraints achievable with the present data, though they remain subject to uncertainties stemming from the limited precision of volatile measurements in the Earth's deep mantle. Continued advances in mantle thermodynamic modeling would help refine our results in the future.

ACKNOWLEDGMENTS

EJL thanks Curtis Williams whose seminar at McGill and follow-up discussions helped spark the project. Huiyi (Cheryl) Wang carried out some of the initial calculations, for which Nicolas Cowan and William Minarik provided feedback. We thank James Day, Steve Desch, Ruth Murray-Clay, James Owen, and Rita Parai for insightful discussions. Some of these discussions took place at the KITP Edgeplanets program in 2025, supported in part by grant NSF PHY-2309135 to the Kavli Institute for Theoretical Physics (KITP). VS acknowledges support by the Fonds de recherche du Québec - Nature et technologies (FRQNT) Master's Training Scholarships and by the Natural Sciences and Engineering Research Council of Canada (NSERC) Postgraduate Scholarship - Doctoral (PGS D). EJL was supported by NSF Research Grant 2509275, NSERC Discovery Grant RGPIN-2020-07045, DGECR-2020-00230, FRQNT Établissement de la relève professorale FRQ-NT NC-298962, FRQNT/NSERC NOVA Grant FRQ-NT 2023-NOVA-325929, NSERC ALLRP 577027-22, and the William Dawson Scholarship from McGill University. Computations were performed on the Graham, Cedar and Rorqual clusters of the Digital Research Alliance of Canada, along with the Triton Shared Computing Cluster (TSCC) of the San Diego Supercomputer Center.

AUTHOR CONTRIBUTIONS

VS carried out all the calculations and drafted the writing. EJL conceived the project and supervised the overall calculations and writing.

REFERENCES

Abe, Y., & Matsui, T. 1985, Lunar and Planetary Science Conference Proceedings, 90, C545

Agnor, C. B., Canup, R. M., & Levison, H. F. 1999, Icarus, 142, 219, doi: https://doi.org/10.1006/icar.1999.6201

Alaerts, L., Lewis, R. S., & Anders, E. 1979a, GeoCoA, 43, 1399, doi: 10.1016/0016-7037(79)90134-0

Alaerts, L., Lewis, R. S., & Anders, E. 1979b, GeoCoA, 43, 1421, doi: 10.1016/0016-7037(79)90136-4

Cieza, L. 2014, in Protostars and Planets VI, ed. H. Beuther, R. S. Klessen, C. P. Dullemond, &

Alexander, R., Pascucci, I., Andrews, S., Armitage, P., &

T. Henning, 475–496,

doi: 10.2458/azu_uapress_9780816531240-ch021

Anders, E., & Grevesse, N. 1989, Geochimica et Cosmochimica Acta, 53, 197,

doi: https://doi.org/10.1016/0016-7037(89)90286-X

- Anderson, W. W., & Ahrens, T. J. 1994, J. Geophys. Res., 99, 4273, doi: 10.1029/93JB03158
- Asplund, M., Amarsi, A. M., & Grevesse, N. 2021, A&A, 653, A141, doi: 10.1051/0004-6361/202140445
- Bailey, A., & Zhu, Z. 2023, arXiv e-prints, arXiv:2310.03117, doi: 10.48550/arXiv.2310.03117
- Ballentine, C. J., & Barfod, D. N. 2000, Earth and Planetary Science Letters, 180, 39, doi: https://doi.org/10.1016/S0012-821X(00)00161-8
- Ballentine, C. J., Marty, B., Sherwood Lollar, B., & Cassidy, M. 2005, Nature, 433, 33, doi: 10.1038/nature03182
- Bekaert, D. V., Broadley, M. W., & Marty, B. 2020,Scientific Reports, 10, 5796,doi: 10.1038/s41598-020-62650-3
- Bender, M. L., Barnett, B., Dreyfus, G., Jouzel, J., & Porcelli, D. 2008, Proceedings of the National Academy of Science, 105, 8232, doi: 10.1073/pnas.0711679105
- Benvenuto, O. G., Fortier, A., & Brunini, A. 2009, Icarus, 204, 752, doi: 10.1016/j.icarus.2009.07.003
- Bernatowicz, T. J., & Fahey, A. J. 1986, GeoCoA, 50, 445, doi: 10.1016/0016-7037(86)90197-3
- Béthune, W., & Rafikov, R. R. 2019, MNRAS, 488, 2365, doi: 10.1093/mnras/stz1870
- Bianchi, D., Sarmiento, J. L., Gnanadesikan, A., et al. 2010, Earth and Planetary Science Letters, 297, 379, doi: 10.1016/j.epsl.2010.06.037
- Binney, J., & Tremaine, S. 2008, Galactic Dynamics: Second Edition, 643–655
- Birch, F. 1964, J. Geophys. Res., 69, 4377, doi: 10.1029/JZ069i020p04377
- Bird, R. B., Stewart, W. E., & Lightfoot, E. N. 2007, Transport Phenomena, revised 2nd edn. (New York: John Wiley & Sons)
- Brasser, R. 2025, A&A, 694, A318, doi: 10.1051/0004-6361/202452394
- Broadley, M. W., Barry, P. H., Bekaert, D. V., et al. 2020, Proceedings of the National Academy of Science, 117, 13997, doi: 10.1073/pnas.2003907117
- Busemann, H., Baur, H., & Wieler, R. 2000, M&PS, 35, 949, doi: 10.1111/j.1945-5100.2000.tb01485.x
- Cameron, A. G. W., & Ward, W. R. 1976, in Lunar and Planetary Science Conference, Vol. 7, Lunar and Planetary Science Conference, 120
- Canup, R. M. 2004, ARA&A, 42, 441, doi: 10.1146/annurev.astro.41.082201.113457
- Canup, R. M. 2008, Icarus, 196, 518, doi: 10.1016/j.icarus.2008.03.011
- Canup, R. M. 2012, Science, 338, 1052, doi: 10.1126/science.1226073

- Canup, R. M., & Asphaug, E. 2001, Nature, 412, 708, doi: 10.1038/35089010
- Chambers, J. 2006, Icarus, 180, 496, doi: https://doi.org/10.1016/j.icarus.2005.10.017
- Colin, A., Moreira, M., Gautheron, C., & Burnard, P. 2015, Chemical Geology, 417, 173, doi: 10.1016/j.chemgeo.2015.09.020
- Ćuk, M., & Stewart, S. T. 2012, Science, 338, 1047, doi: 10.1126/science.1225542
- D'Angelo, G., Weidenschilling, S. J., Lissauer, J. J., & Bodenheimer, P. 2021, Icarus, 355, 114087,
 doi: 10.1016/j.icarus.2020.114087
- Dauphas, N. 2003, Icarus, 165, 326, doi: 10.1016/S0019-1035(03)00198-2
- Dauphas, N. 2017, Nature, 541, 521, doi: 10.1038/nature20830
- Dauphas, N., & Pourmand, A. 2011, Nature, 473, 489, doi: 10.1038/nature10077
- Day, J. M., Barry, P. H., Hilton, D. R., et al. 2015,
 Geochimica et Cosmochimica Acta, 153, 116,
 doi: https://doi.org/10.1016/j.gca.2015.01.008
- Day, J. M., Jones, T. D., & Nicklas, R. W. 2022, Chemical Geology, 587, 120626,
 doi: https://doi.org/10.1016/j.chemgeo.2021.120626
- Day, J. M. D., Hilton, D. R., Pearson, D. G., et al. 2005, Geology, 33, 733, doi: 10.1130/G21625.1
- Day, J. M. D., & Moynier, F. 2014, Philosophical Transactions of the Royal Society of London Series A, 372, 20130259, doi: 10.1098/rsta.2013.0259
- Desch, S. J., & Robinson, K. L. 2019, Geochemistry, 79, 125546,
 - doi: https://doi.org/10.1016/j.chemer.2019.125546
- Dodds, K. H., Bryson, J. F. J., Neufeld, J. A., & Harrison,
 R. J. 2021, Journal of Geophysical Research (Planets),
 126, e06704, doi: 10.1029/2020JE006704
- Elkins-Tanton, L. 2008, Earth and Planetary Science Letters, 271, 181,
- doi: https://doi.org/10.1016/j.epsl.2008.03.062
- Elkins-Tanton, L. T. 2012, Annual Review of Earth and Planetary Sciences, 40, 113,
 - ${\bf doi:\ 10.1146/annurev-earth-042711-105503}$
- Farley, K., Maier-Reimer, E., Schlosser, P., & Broecker, W. 1995, Journal of geophysical research, 100, 3829, doi: 10.1029/94JB02913
- Ferguson, J. W., Alexander, D. R., Allard, F., et al. 2005, ApJ, 623, 585, doi: 10.1086/428642
- Freedman, R. S., Lustig-Yaeger, J., Fortney, J. J., et al. 2014, ApJS, 214, 25, doi: 10.1088/0067-0049/214/2/25
- Genda, H. 2016, GEOCHEMICAL JOURNAL, 50, 27, doi: 10.2343/geochemj.2.0398

- Genda, H., & Ikoma, M. 2008, Icarus, 194, 42, doi: 10.1016/j.icarus.2007.09.007
- Grevesse, N., & Noels, A. 1993, in Origin and Evolution of the Elements, ed. N. Prantzos, E. Vangioni-Flam, & M. Casse, 15–25
- Halliday, A. N. 2000, Earth and Planetary Science Letters, 176, 17, doi: 10.1016/S0012-821X(99)00317-9
- Halliday, A. N. 2008, Philosophical Transactions of the Royal Society of London Series A, 366, 4163, doi: 10.1098/rsta.2008.0209
- Halliday, A. N. 2013, GeoCoA, 105, 146, doi: 10.1016/j.gca.2012.11.015
- Hansen, B. M. S. 2009, ApJ, 703, 1131, doi: 10.1088/0004-637X/703/1/1131
- Harper, Jr., C. L., & Jacobsen, S. B. 1996, Science, 273, 1814, doi: 10.1126/science.273.5283.1814
- Hartmann, W. K., & Davis, D. R. 1975, Icarus, 24, 504, doi: 10.1016/0019-1035(75)90070-6
- Hayashi, C. 1981, Progress of Theoretical Physics Supplement, 70, 35, doi: 10.1143/PTPS.70.35
- Hayashi, C., Nakazawa, K., & Nakagawa, Y. 1985, in Protostars and Planets II, ed. D. C. Black & M. S. Matthews, 1100–1153
- Heber, V. S., Baur, H., Bochsler, P., et al. 2012, ApJ, 759, 121, doi: 10.1088/0004-637X/759/2/121
- Hilton, D. R., Grönvold, K., Macpherson, C. G., & Castillo,
 P. R. 1999, Earth and Planetary Science Letters, 173, 53,
 doi: 10.1016/S0012-821X(99)00215-0
- Hirschmann, M. M. 2000, Geochemistry, Geophysics, Geosystems, 1, 1042, doi: 10.1029/2000GC000070
- Hohenberg, C. M., Thonnard, N., & Meshik, A. 2002, M&PS, 37, 257, doi: 10.1111/j.1945-5100.2002.tb01108.x
- Holland, G., & Ballentine, C. J. 2006, Nature, 441, 186, doi: 10.1038/nature04761
- Holland, G., Cassidy, M., & Ballentine, C. J. 2009, Science, 326, 1522, doi: 10.1126/science.1179518
- Huss, G. R., Lewis, R. S., & Hemkin, S. 1996, GeoCoA, 60, 3311, doi: 10.1016/0016-7037(96)00168-8
- Iacono-Marziano, G., Paonita, A., Rizzo, A., Scaillet, B., & Gaillard, F. 2010, Chemical Geology, 279, 145, doi: https://doi.org/10.1016/j.chemgeo.2010.10.017
- Ida, S., & Lin, D. N. C. 2004, The Astrophysical Journal, 604, 388, doi: 10.1086/381724
- Ida, S., & Makino, J. 1993, Icarus, 106, 210, doi: 10.1006/icar.1993.1167
- Ikoma, M., Nakazawa, K., & Emori, H. 2000, ApJ, 537, 1013, doi: 10.1086/309050
- Izidoro, A., Bitsch, B., & Dasgupta, R. 2021, ApJ, 915, 62, doi: 10.3847/1538-4357/abfe0b

- Jackson, M. G., Kurz, M. D., & Hart, S. R. 2009, Earth and Planetary Science Letters, 287, 519, doi: https://doi.org/10.1016/j.epsl.2009.08.039
- Jacobson, S. A., & Morbidelli, A. 2014, Philosophical Transactions of the Royal Society of London Series A, 372, 0174, doi: 10.1098/rsta.2013.0174
- Jambon, A., Weber, H., & Braun, O. 1986, Geochimica et Cosmochimica Acta, 50, 401,
 - doi: https://doi.org/10.1016/0016-7037(86)90193-6
- Jaupart, E., Charnoz, S., & Moreira, M. 2017, Icarus, 293, 199, doi: 10.1016/j.icarus.2017.04.022
- Jeanloz, R. 1979, J. Geophys. Res., 84, 6059, doi: 10.1029/JB084iB11p06059
- Jephcoat, A., & Olson, P. 1987, Nature, 325, 332, doi: 10.1038/325332a0
- Johansen, A., & Lacerda, P. 2010, MNRAS, 404, 475, doi: 10.1111/j.1365-2966.2010.16309.x
- Johansen, A., Ronnet, T., Bizzarro, M., et al. 2021, Science Advances, 7, eabc0444, doi: 10.1126/sciadv.abc0444
- Kaib, N. A., & Chambers, J. E. 2016, MNRAS, 455, 3561, doi: 10.1093/mnras/stv2554
- Kaib, N. A., & Cowan, N. B. 2015, Icarus, 252, 161, doi: 10.1016/j.icarus.2015.01.013
- Kallemeyn, G. W., Rubin, A. E., & Wasson, J. T. 1994, GeoCoA, 58, 2873, doi: 10.1016/0016-7037(94)90121-X
- Kallemeyn, G. W., & Wasson, J. T. 1981, GeoCoA, 45, 1217, doi: 10.1016/0016-7037(81)90145-9
- Kaminski, E., Limare, A., Kenda, B., & Chaussidon, M. 2020, Earth and Planetary Science Letters, 548, 116469, doi: https://doi.org/10.1016/j.epsl.2020.116469
- Kendrick, M. A., Scambelluri, M., Hermann, J., & Padrón-Navarta, J. A. 2018, Geochimica et Cosmochimica Acta, 235, 285, doi: https://doi.org/10.1016/j.gca.2018.03.024
- Kendrick, M. A., Scambelluri, M., Honda, M., & Phillips, D. 2011, Nature Geoscience, 4, 807, doi: 10.1038/ngeo1270
- Kleine, T., Touboul, M., Bourdon, B., et al. 2009, GeoCoA, 73, 5150, doi: 10.1016/j.gca.2008.11.047
- Kokubo, E., & Ida, S. 2000, Icarus, 143, 15, doi: https://doi.org/10.1006/icar.1999.6237
- Kruijer, T. S., & Kleine, T. 2017, Earth and Planetary Science Letters, 475, 15, doi: 10.1016/j.epsl.2017.07.021
- Kurz, M. D., Curtice, J., Fornari, D., Geist, D., & Moreira, M. 2009, Earth and Planetary Science Letters, 286, 23, doi: 10.1016/j.epsl.2009.06.008
- Laibe, G., Gonzalez, J. F., & Maddison, S. T. 2012, A&A, 537, A61, doi: 10.1051/0004-6361/201015349
- Lambrechts, M., & Lega, E. 2017, A&A, 606, A146, doi: 10.1051/0004-6361/201731014

- Larrodera, C., & Cid, C. 2020, A&A, 635, A44, doi: 10.1051/0004-6361/201937307
- Lee, E. J., & Chiang, E. 2016, ApJ, 817, 90, doi: 10.3847/0004-637X/817/2/90
- Lee, E. J., Chiang, E., & Ormel, C. W. 2014, The Astrophysical Journal, 797, 95, doi: 10.1088/0004-637x/797/2/95
- Lewis, R. S., Srinivasan, B., & Anders, E. 1975, Science, 190, 1251
- Lodders, K. 2003, ApJ, 591, 1220, doi: 10.1086/375492
- Lugmair, G., & Shukolyukov, A. 1998, Geochimica et Cosmochimica Acta, 62, 2863,
 - doi: https://doi.org/10.1016/S0016-7037(98)00189-6
- Lupton, J., & Craig, H. 1975, Earth and Planetary Science Letters, 26, 133,
 - doi: https://doi.org/10.1016/0012-821X(75)90080-1
- Mamajek, E. E. 2009, in American Institute of Physics
 Conference Series, Vol. 1158, Exoplanets and Disks:
 Their Formation and Diversity, ed. T. Usuda,
 M. Tamura, & M. Ishii, 3–10, doi: 10.1063/1.3215910
- Marrocchi, Y., Marty, B., Reinhardt, P., & Robert, F. 2011, GeoCoA, 75, 6255, doi: 10.1016/j.gca.2011.07.048
- Marty, B. 2012, Earth and Planetary Science Letters, 313, 56, doi: 10.1016/j.epsl.2011.10.040
- Marty, B. 2020, Geochemical Perspectives, 9, 176, doi: 10.7185/geochempersp.9.2
- Marty, B. 2022, Icarus, 381, 115020, doi: https://doi.org/10.1016/j.icarus.2022.115020
- Mastrobuono-Battisti, A., Perets, H. B., & Raymond, S. N. 2015, Nature, 520, 212, doi: 10.1038/nature14333
- Meier, M., Reufer, A., & Wieler, R. 2014, Icarus, 242, 316, doi: https://doi.org/10.1016/j.icarus.2014.08.003
- Michel, A., van der Marel, N., & Matthews, B. C. 2021, ApJ, 921, 72, doi: 10.3847/1538-4357/ac1bbb
- Mizuno, H., Nakazawa, K., & Hayashi, C. 1980, Earth and Planetary Science Letters, 50, 202,
- doi: https://doi.org/10.1016/0012-821X(80)90131-4
- Moldenhauer, T. W., Kuiper, R., Kley, W., & Ormel, C. W. 2021, A&A, 646, L11, doi: 10.1051/0004-6361/202040220
- Morbidelli, A., Kleine, T., & Nimmo, F. 2025, Earth and Planetary Science Letters, 650, 119120, doi: 10.1016/j.epsl.2024.119120
- Mordasini, C. 2014, A&A, 572, A118, doi: 10.1051/0004-6361/201423702
- Mordasini, C., Klahr, H., Alibert, Y., Miller, N., & Henning, T. 2014, A&A, 566, A141, doi: 10.1051/0004-6361/201321479
- Moreira, M. 2013, Geochemical Perspectives, 2, 229, doi: 10.7185/geochempersp.2.2

- Moreira, M., & Charnoz, S. 2016, Earth and Planetary Science Letters, 433, 249, doi: https://doi.org/10.1016/j.epsl.2015.11.002
- Morgan, J. W., Walker, R. J., Brandon, A. D., & Horan, M. F. 2001, M&PS, 36, 1257, doi: 10.1111/j.1945-5100.2001.tb01959.x
- Mukhopadhyay, S., & Parai, R. 2019, Annual Review of Earth and Planetary Sciences, 47, 389,
 - doi: 10.1146/annurev-earth-053018-060238
- Nakagawa, Y., Sekiya, M., & Hayashi, C. 1986, Icarus, 67, 375, doi: https://doi.org/10.1016/0019-1035(86)90121-1
- Okuchi, T. 1997, Science, 278, 1781, doi: 10.1126/science.278.5344.1781
- Onyett, I. J., Schiller, M., Makhatadze, G. V., et al. 2023, Nature, 619, 539, doi: 10.1038/s41586-023-06135-z
- Ormel, C. W. 2014, ApJL, 789, L18, doi: 10.1088/2041-8205/789/1/L18
- Ormel, C. W., & Klahr, H. H. 2010, A&A, 520, A43, doi: 10.1051/0004-6361/201014903
- Ott, U. 2002, Reviews in Mineralogy and Geochemistry, 47, 71, doi: 10.2138/rmg.2002.47.3
- O'Brien, D. P., Walsh, K. J., Morbidelli, A., Raymond, S. N., & Mandell, A. M. 2014, Icarus, 239, 74, doi: https://doi.org/10.1016/j.icarus.2014.05.009
- Papaloizou, J. C. B., & Larwood, J. D. 2000, MNRAS, 315, 823, doi: 10.1046/j.1365-8711.2000.03466.x
- Parai, R. 2022, Proceedings of the National Academy of Science, 119, e2201815119, doi: 10.1073/pnas.2201815119
- Pepin, R. O. 1991, Icarus, 92, 2, doi: 10.1016/0019-1035(91)90036-S
- Pepin, R. O. 1997, Icarus, 126, 148, doi: 10.1006/icar.1996.5639
- Pepin, R. O., & Porcelli, D. 2002, Reviews in Mineralogy and Geochemistry, 47, 191, doi: 10.2138/rmg.2002.47.7
- Peron, S., Moreira, M., & Agranier, A. 2018, Geochemistry, Geophysics, Geosystems, 19, 979, doi: 10.1002/2017GC007388
- Peron, S., Moreira, M., Colin, A., et al. 2016, Earth and Planetary Science Letters, 449, 145, doi: 10.1016/j.epsl.2016.05.052
- Peron, S., Moreira, M., Putlitz, B., & Kurz, M. D. 2017, Geochemical Perspectives Letters, 3, 151, doi: 10.7185/geochemlet.1718
- Peron, S., & Mukhopadhyay, S. 2022, Earth and Planetary Science Letters, 593, 117655,
- doi: https://doi.org/10.1016/j.epsl.2022.117655
- Piso, A.-M. A., & Youdin, A. N. 2014, ApJ, 786, 21, doi: 10.1088/0004-637X/786/1/21
- Piso, A.-M. A., Youdin, A. N., & Murray-Clay, R. A. 2015, ApJ, 800, 82, doi: 10.1088/0004-637X/800/2/82

- Poirier, J.-P. 1994, Physics of the Earth and Planetary Interiors, 85, 319,
 - doi: https://doi.org/10.1016/0031-9201(94)90120-1
- Pollack, J. B., Hubickyj, O., Bodenheimer, P., et al. 1996,Icarus, 124, 62, doi: 10.1006/icar.1996.0190
- Ponganis, K. V., Graf, T., & Marti, K. 1997,
- J. Geophys. Res., 102, 19335, doi: 10.1029/97JE01686
 Popovas, A., Nordlund, Å., Ramsey, J. P., & Ormel, C. W.
- 2018, Monthly Notices of the Royal Astronomical Society, 479, 5136, doi: 10.1093/mnras/sty1752
- Porcelli, D., Woolum, D., & Cassen, P. 2001, Earth and Planetary Science Letters, 193, 237, doi: 10.1016/S0012-821X(01)00493-9
- Priestley, C. H. B. 1957, Proceedings of the Royal Society of London Series A, 238, 287, doi: 10.1098/rspa.1957.0001
- Priestley, C. H. B. 1959, Quarterly Journal of the Royal Meteorological Society, 85, 415, doi: 10.1002/qj.49708536611
- Pujol, M., Marty, B., & Burgess, R. 2011, Earth and Planetary Science Letters, 308, 298, doi: 10.1016/j.epsl.2011.05.053
- Péron, S., Mukhopadhyay, S., Kurz, M. D., & Graham,D. W. 2021, Nature, 600, 462,doi: 10.1038/s41586-021-04092-z
- Quarles, B. L., & Lissauer, J. J. 2015, Icarus, 248, 318, doi: 10.1016/j.icarus.2014.10.044
- Rafikov, R. R. 2017, ApJ, 837, 163, doi: 10.3847/1538-4357/aa6249
- Raquin, A., & Moreira, M. 2009, Earth and Planetary Science Letters, 287, 551, doi: 10.1016/j.epsl.2009.09.003
- Raymond, S. N., & Izidoro, A. 2017, Icarus, 297, 134, doi: 10.1016/j.icarus.2017.06.030
- Raymond, S. N., O'Brien, D. P., Morbidelli, A., & Kaib,
 N. A. 2009, Icarus, 203, 644,
 doi: https://doi.org/10.1016/j.icarus.2009.05.016
- Ricard, Y., Bercovici, D., & Albarède, F. 2017, Icarus, 285, 103, doi: https://doi.org/10.1016/j.icarus.2016.12.020
- Rodenkirch, P. J., & Dullemond, C. P. 2022, A&A, 659, A42, doi: 10.1051/0004-6361/202142571
- Rudge, J. F., Kleine, T., & Bourdon, B. 2010, Nature Geoscience, 3, 439, doi: 10.1038/ngeo872
- Safronov, V. S. 1972, Evolution of the protoplanetary cloud and formation of the earth and planets.
- Safronov, V. S., & Zvjagina, E. V. 1969, Icarus, 10, 109, doi: 10.1016/0019-1035(69)90013-X
- Sander, R. 2015, Atmospheric Chemistry & Physics, 15, 4399, doi: 10.5194/acp-15-4399-201510.5194/acpd-14-29615-2014
- Sanloup, C., Schmidt, B. C., Perez, E. M. C., et al. 2005, Science, 310, 1174, doi: 10.1126/science.1119070

- Sano, Y., Nakamura, Y., Notsu, K., & Wakita, H. 1988,GeoCoA, 52, 1305, doi: 10.1016/0016-7037(88)90284-0
- Sasaki, S., & Nakazawa, K. 1990, Icarus, 85, 21, doi: https://doi.org/10.1016/0019-1035(90)90101-E
- Savignac, V., & Lee, E. J. 2024, ApJ, 973, 85, doi: 10.3847/1538-4357/ad6317
- Scott, E., & Krot, A. 2007, in Treatise on Geochemistry, ed. H. D. Holland & K. K. Turekian (Oxford: Pergamon), 1–72,
 - doi: https://doi.org/10.1016/B0-08-043751-6/01145-2
- Sharp, Z. D. 2017, Chemical Geology, 448, 137, doi: https://doi.org/10.1016/j.chemgeo.2016.11.018
- Solomatov, V. S. 2000, in Origin of the Earth and Moon, ed. R. M. Canup, K. Righter, & et al., 323–338
- Solomatov, V. S., & Moresi, L. N. 2000, J. Geophys. Res., 105, 21795, doi: 10.1029/2000JB900197
- Sorokhtin, O., Chilingar, G., & Sorokhtin, N. 2011, in Developments in Earth and Environmental Sciences, Vol. 10, Evolution of Earth and its Climate: Birth, Life and Death of Earth, ed. O. Sorokhtin, G. Chilingarian, & N. Sorokhtin (Elsevier), 13–60,
- doi: https://doi.org/10.1016/B978-0-444-53757-7.00002-7
- Stixrude, L., Wasserman, E., & Cohen, R. E. 1997,
 J. Geophys. Res., 102, 24,729, doi: 10.1029/97JB02125
- Tabata, T., & Shirai, T. 2000, Atomic Data and Nuclear Data Tables, 76, 1,
 - doi: https://doi.org/10.1006/adnd.2000.0835
- Tanaka, H., Takeuchi, T., & Ward, W. R. 2002, ApJ, 565, 1257, doi: 10.1086/324713
- Tomlinson, E. L., & Holland, T. J. B. 2021, Journal of Petrology, 62, egab012, doi: 10.1093/petrology/egab012
- Trieloff, M., & Kunz, J. 2005, Physics of the Earth and Planetary Interiors, 148, 13, doi: https://doi.org/10.1016/j.pepi.2004.07.007
- Trieloff, M., Kunz, J., Clague, D. A., Harrison, D., & Allègre, C. J. 2000, Science, 288, 1036, doi: 10.1126/science.288.5468.1036
- Tucker, J. M., & Mukhopadhyay, S. 2014, Earth and Planetary Science Letters, 393, 254, doi: 10.1016/j.epsl.2014.02.050
- Valbracht, P. J., Staudacher, T., Malahoff, A., & Allègre,
 C. J. 1997, Earth and Planetary Science Letters, 150,
 399, doi: 10.1016/S0012-821X(97)00094-0
- Valencia, D., O'Connell, R. J., & Sasselov, D. 2006, Icarus, 181, 545,
 - doi: https://doi.org/10.1016/j.icarus.2005.11.021
- Walker, R. J. 2009, Chemie der Erde / Geochemistry, 69, 101, doi: 10.1016/j.chemer.2008.10.001
- Walsh, K. J., & Levison, H. F. 2016, The Astronomical Journal, 152, 68, doi: 10.3847/0004-6256/152/3/68

- Walsh, K. J., & Levison, H. F. 2019, Icarus, 329, 88, doi: 10.1016/j.icarus.2019.03.031
- Walsh, K. J., Morbidelli, A., Raymond, S. N., O'Brien, D. P., & Mandell, A. M. 2011, Nature, 475, 206, doi: 10.1038/nature10201
- Wang, K., Lu, X., Liu, X., Zhou, M., & Yin, K. 2022, Geochimica et Cosmochimica Acta, 321, 329, doi: https://doi.org/10.1016/j.gca.2022.01.009
- Weidenschilling, S. J. 1977, MNRAS, 180, 57, doi: 10.1093/mnras/180.2.57
- Weidenschilling, S. J., Spaute, D., Davis, D. R., Marzari, F., & Ohtsuki, K. 1997, Icarus, 128, 429, doi: 10.1006/icar.1997.5747
- Wetherill, G. W. 1975, Lunar and Planetary Science Conference Proceedings, 2, 1539
- Wetherill, G. W., & Stewart, G. R. 1989, Icarus, 77, 330, doi: 10.1016/0019-1035(89)90093-6
- Wiechert, U., Halliday, A. N., Lee, D. C., et al. 2001, Science, 294, 345, doi: 10.1126/science.1063037

- Wieler, R., Anders, E., Baur, H., Lewis, R. S., & Signer, P. 1992, GeoCoA, 56, 2907,
 - doi: 10.1016/0016-7037(92)90367-R
- Wieler, R., Baur, H., Signer, P., Anders, E., & Lewis, R. S. 1991, GeoCoA, 55, 1709, doi: 10.1016/0016-7037(91)90141-Q.
- Williams, C. D., & Mukhopadhyay, S. 2019, Nature, 565, 78, doi: 10.1038/s41586-018-0771-1
- Young, C. J., & Lay, T. 1987, Annual Review of Earth and Planetary Sciences, 15, 25, doi: 10.1146/annurev.ea.15.050187.000325
- Young, E. D., Shahar, A., & Schlichting, H. E. 2023, Nature, 616, 306, doi: 10.1038/s41586-023-05823-0
- Zhang, J., Dauphas, N., Davis, A. M., Leya, I., & Fedkin,
 A. 2012, Nature Geoscience, 5, 251,
 doi: 10.1038/ngeo1429
- Zhou, J.-L., Lin, D. N. C., & Sun, Y.-S. 2007, ApJ, 666, 423, doi: 10.1086/519918
- Zhu, Z., Jiang, Y.-F., Baehr, H., et al. 2021, Monthly Notices of the Royal Astronomical Society, 508, 453, doi: 10.1093/mnras/stab2517